

M²RNN: Non-Linear RNNs with Matrix-Valued States for Scalable Language Modeling

Mayank Mishra^{1,2}, Shawn Tan³, Ion Stoica¹, Joseph Gonzalez^{1*}, Tri Dao^{4,5*}

¹UC Berkeley, ²Learning Machine, ³MIT-IBM Watson Lab, ⁴Princeton University, ⁵Together AI

*Equal Mentoring

Transformers are highly parallel but are limited to computations in the \mathbf{TC}^0 complexity class, excluding tasks such as entity tracking and code execution that provably require greater expressive power. Motivated by this limitation, we revisit non-linear Recurrent Neural Networks (RNNs) for language modeling and introduce Matrix-to-Matrix RNN (M²RNN): an architecture with matrix-valued hidden states and expressive non-linear state transitions. We demonstrate that the language modeling performance of non-linear RNNs is limited by their state size. We also demonstrate how the state size expansion mechanism enables efficient use of tensor cores. Empirically, M²RNN achieves perfect state tracking generalization at sequence lengths not seen during training. These benefits also translate to large-scale language modeling. In hybrid settings that interleave recurrent layers with attention, Hybrid M²RNN outperforms equivalent Gated DeltaNet hybrids by 0.4–0.5 perplexity points on a 7B MoE model, while using 3× smaller state sizes for the recurrent layers. Notably, replacing even a single recurrent layer with M²RNN in an existing hybrid architecture yields accuracy gains comparable to Hybrid M²RNN with minimal impact on training throughput. Further, the Hybrid Gated DeltaNet models with a single M²RNN layer also achieve superior long-context generalization, outperforming state-of-the-art hybrid linear attention architectures by up to 8 points on LongBench. Together, these results establish non-linear RNN layers as a compelling building block for efficient and scalable language models.

Correspondence: Mayank Mishra @ mayank@learning-machine.ai

Training Code: <https://github.com/open-lm-engine/lm-engine>

Kernels: <https://github.com/open-lm-engine/accelerated-model-architectures>

Models: <https://huggingface.co/collections/open-lm-engine/m2rnn>

1 Introduction

Foundation models trained on massive datasets and adapted to downstream tasks have become the dominant paradigm in modern machine learning (Brown et al., 2020; Chowdhery et al., 2023; Grattafori et al., 2024). At their core, these models rely on sequence-based architectures capable of processing diverse modalities including text, code, images, video, and speech (Brown et al., 2020; Chowdhery et al., 2023; Grattafori et al., 2024; Mishra et al., 2024; Dosovitskiy, 2020; Lugosch et al., 2019). The prevailing architecture is the decoder-only Transformer, composed of alternating multi-layer perceptron (MLP) and causal attention layers (Vaswani et al., 2017). Much of attention’s success stems from its amenability to parallelization across the sequence length, the availability of hardware-efficient implementations (Dao et al., 2022; Dao, 2023; Shah et al., 2024; Zadouri et al., 2026), and its effective in-context retrieval capabilities. Attention-based Transformers have also demonstrated remarkable scalability, powering models ranging from hundreds of billions (Brown et al., 2020; Chowdhery et al., 2023; Workshop et al., 2022; Smith et al., 2022; Liu et al., 2024; Yang et al., 2025) to trillions of parameters (Team et al., 2025; Meta AI, 2025).

However, attention’s quadratic time complexity during training and linearly growing memory requirements during inference have motivated the development of more efficient alternatives (Tay et al., 2022). State Space Models (SSMs) and linear attention (Gu et al., 2021a,b; Gu and Dao, 2024; Dao and Gu, 2024; Yang et al., 2023, 2024b,a; Peng et al., 2023) have emerged as promising replacements. Katharopoulos et al. (2020) propose computing linear attention via a dot product of kernel features, Peng et al. (2021) approximate attention using random feature methods, Schlag et al. (2021) introduce the delta update rule, showing significant improvements in associative recall, and Gu and Dao (2024); Dao and Gu (2024) propose Mamba with an efficient training algorithm that scales linearly with sequence length.

Linear attention admits both a recurrent and a parallel formulation. The constant-state size for linear attention enables memory-efficient and fast autoregressive inference (using the recurrent form) while the standard parallel form retains quadratic complexity during training. To bridge this gap, a chunkwise parallel formulation can be employed (Hua et al., 2022; Yang et al., 2023), preserving linear time complexity while batching computations within chunks to leverage matrix multiplication units (tensor cores on NVIDIA GPUs (NVIDIA Corporation)). SSMs like Mamba-1 (Gu and Dao, 2024) can alternatively be accelerated via the parallel scan algorithm (Hillis and Steele, 1986; Blelloch, 1990).

Although linear RNNs have attracted considerable attention due to their efficient inference and training, they present several notable limitations:

1. **Limited state tracking:** Linear RNNs are provably less expressive than non-linear RNNs, particularly for hard state-tracking tasks such as code evaluation, entity tracking, and permutation composition (S_5 group permutation task). Consequently, they are no more expressive than Transformers (Merrill et al., 2024).
2. **Poor in-context retrieval performance:** Linear RNNs exhibit weak performance in in-context retrieval tasks (Yang et al., 2023, 2024b,a). Because their recurrent state is updated via a fixed-rank outer product, the state can be overwritten when the number of key-value associations exceeds its capacity, leading to degraded in-context retrieval performance. This manifests as poor performance on needle-in-a-haystack benchmarks and long-context recall tasks that require retrieving specific information from distant context.

A common strategy is to interleave quadratic attention layers with sub-quadratic recurrent layers in order to achieve a balance between inference efficiency and downstream task performance in state-of-the-art production models. This alleviates the poor language modeling and long-context performance of linear RNNs while retaining their long-context training and inference efficiency advantages (Blakeman et al., 2025; Lieber et al., 2024; Ren et al., 2024).

While non-linear RNNs have been shown to excel at hard state tracking problems (Merrill et al., 2024), they face several practical challenges:

1. **Poor language modeling performance:** Current non-linear RNNs significantly underperform linear RNNs in language modeling. We show that large state sizes are critical for strong language modeling performance, and that the inferior results of non-linear RNNs are primarily due to their smaller state sizes rather than their non-linearity.
2. **Poor long-context retrieval performance:** We further show that the smaller state sizes significantly hurt the retrieval and long-context performance. The vector-valued non-linear RNNs in our experiments consistently underperform Mamba-2 and Gated DeltaNet by ≈ 20 points in real-world retrieval tasks (Tables 3, 4).
3. **Training inefficiency:** Unlike linear RNNs, non-linear RNNs cannot be parallelized across the sequence length, making training significantly more expensive. This is compounded by poor hardware utilization: naïve recurrent GEMM execution prevents reuse of on-chip tiles across time steps, forcing costly HBM I/O and synchronization. Even block-wise variants (Pöppel et al., 2025) remain constrained by micro-batch tiling, leading to padding overhead and wasted FLOPs.

We propose Matrix-to-Matrix RNN (M²RNN), a non-linear RNN architecture that when combined with Hybrid linear RNNs results in a significant performance improvement in both language modeling and long-

context performance. Specifically, M²RNN layers address the following key limitations of linear RNNs and non-linear RNNs:

1. **Improved state tracking:** Matrix-to-Matrix RNN (M²RNN) layer achieves perfect state tracking, significantly improving state tracking performance over linear RNNs similar to non-linear RNNs and GRUs (Cho et al., 2014a). We further demonstrate that M²RNN layers can express all computations that can be performed by a non-linear RNN.
2. **Improved language modeling, in-context retrieval and long-context performance:** We demonstrate the importance of large state sizes for recurrent models and that it is a key driver behind the success of linear RNNs such as Mamba-2 (Dao and Gu, 2024) and Gated DeltaNet (Yang et al., 2024a). We show that the outer product state expansion mechanism is directly applicable to non-linear RNNs. Similar to LSTMs (Hochreiter and Schmidhuber, 1997) and GRUs (Cho et al., 2014a), we use a forget gate to prevent gradient degradation across time steps (Chung et al., 2014), but unlike LSTMs and GRUs, our forget gate is independent of the recurrent state, enabling parallel computation. Hybrid M²RNN models outperform Hybrid Mamba-2 and Hybrid Gated DeltaNet on language modeling benchmarks. The outer product state expansion mechanism also improves in-context retrieval and long-context performance which are sensitive to the state size. Further, we demonstrate that combining M²RNN layers with Hybrid Mamba-2 and Hybrid Gated DeltaNet enhances long-context performance by up to 8 points at both 410M dense and 7B MoE scales (Tables 5, 6).
3. **Improved hardware utilization:** The outer product based state expansion mechanism enables efficient tensor core utilization without the wasted FLOPs of FlashRNN (Pöppel et al., 2025) due to padding along the batch dimension (Section 3.4). Since M²RNN layers are computationally expensive and non-parallelizable across time steps, we further explore using M²RNN layers sparingly. We demonstrate with experiments that using M²RNN layers sparingly (even just one layer) results in substantial improvements in all benchmarks.

Beyond efficient single-device execution, training models at scale requires careful attention to systems design. We describe the forward and backward kernels for M²RNN layers implemented in Triton (Tillet et al., 2019), and present two strategies for applying tensor parallelism (TP) to M²RNN layers: a topology-aware approach that requires no additional communication, and a topology-independent approach that preserves parameter count across TP configurations at the cost of extra synchronization (Section 4.3).

2 Background

We use bold letters (**A**) to represent matrices and small letters (*a*) to represent column vectors in the following sections.

2.1 State Tracking

State tracking refers to determining the state of a system by observing a sequence of updates applied to it. The complexity of state tracking tasks is characterized by circuit complexity classes:

TC⁰: **TC⁰** denotes the class of languages decidable by constant-depth threshold boolean circuits of polynomial size. Simple state tracking problems such as parity (equivalent to the permutation group S_2) fall within this class. Merrill et al. (2022) show that Transformers (Vaswani et al., 2017) lie in **TC⁰**, making them capable of solving only these simpler tasks.

NC¹: **NC¹** denotes the class of languages decidable by logarithmic-depth boolean circuits of polynomial size¹. Many practical state tracking tasks such as tracking chess moves or evaluating programs reduce to problems at least as hard as the S_5 word problem, where S_k denotes the symmetric group on k elements (i.e., all permutations of k objects). Since S_5 is **NC¹**-complete, these tasks lie strictly outside the expressivity class of both Transformers (Merrill et al., 2022) and linear SSMS with input-independent or diagonal transition matrices (Merrill et al., 2024), motivating architectures with greater computational expressivity.

¹Depth is measured in the input size.

2.2 Linear RNNs

Both linear attention mechanisms and SSMs admit recurrent and parallel formulations, leading the literature to refer to them collectively as *recurrent neural networks* (RNNs). However, [Merrill et al. \(2024\)](#) demonstrate a significant expressivity gap between these *linear* RNNs and *non-linear* RNNs. Non-linear RNNs, recurrent networks that apply a non-linear activation at each step of the recurrence, have traditionally been employed for sequence modeling ([Elman, 1990](#)), particularly for tasks requiring state tracking across time steps. While the inclusion of a non-linearity yields a much richer class of representable functions, it precludes the use of algorithms like parallel scan ([Hillis and Steele, 1986](#); [Blelloch, 1990](#)) for efficient computation ([Merrill et al., 2024](#)). Nevertheless, the state-tracking capabilities enabled by non-linear RNNs can make their incurred cost a reasonable tradeoff.

Many linear attention and SSM models take the following general form where Equation 1 is used to compute the recurrent state at the next time step and Equation 2 is used to compute the final output:

$$\mathbf{H}_t = \mathbf{H}_{t-1}\mathbf{A}(x_t) + \mathbf{B}(x_t) \quad (1)$$

$$y_t = \mathbf{H}_t^\top c(x_t) + d(x_t) \quad (2)$$

where $\mathbf{H}_t \in \mathbb{R}^{K \times V}$ denotes the recurrent state at time step t , $\mathbf{A}(x_t) \in \mathbb{R}^{V \times V}$ is the transition matrix, and $\mathbf{B}(x_t) \in \mathbb{R}^{K \times V}$ is a function of the input $x_t \in \mathbb{R}^d$. $c(x_t) \in \mathbb{R}^{K \times 1}$ is the vector used to compute the output and $d(x_t) \in \mathbb{R}^{V \times 1}$ is the residual stream. K and V represent the key and value head dimensions respectively. Note that the recurrent state \mathbf{H}_t is a matrix rather than a vector. [Katharopoulos et al. \(2020\)](#) replace the similarity score in attention ($\exp(q_i^\top k_j)$) ([Vaswani et al., 2017](#)) with a kernel $\kappa(q_i, k_j) = \langle \phi(q_i), \phi(k_j) \rangle$ to compute the similarity scores between queries (q_i) and keys (k_j) where ϕ represents the feature map for the kernel function κ . This leads to the following simplified recurrence:

$$\mathbf{H}_t = \mathbf{H}_{t-1} + \phi(k_t)v_t^\top \quad (3)$$

$$z_t = z_{t-1} + \phi(k_t) \quad (4)$$

$$y_t = \frac{\mathbf{H}_t^\top \phi(q_t)}{z_t^\top \phi(q_t)} \quad (5)$$

Prior works found that removing the normalization term in the denominator ($z_t^\top \phi(q_t)$) in Equation 5 improves training stability ([Sun et al., 2023](#)) for linear attention and hence we omit this in going forward. The recurrence then becomes:

$$\mathbf{H}_t = \mathbf{H}_{t-1} + \phi(k_t)v_t^\top \quad (6)$$

$$y_t = \mathbf{H}_t^\top \phi(q_t) \quad (7)$$

A comprehensive summary of recurrent forms for various linear attention models can be found in [Yang et al. \(2024b\)](#) (Table 2).

2.3 Limitations of Linear RNNs

2.3.1 Limited State Tracking

[Merrill et al. \(2024\)](#) demonstrate that hard state tracking tasks like the permutation group S_5 cannot be solved when the transition matrix for a linear RNN is input-independent ($\mathbf{A}(x_t) = \mathbf{A}$) or diagonal ($\mathbf{A}(x_t) = \text{diag}(a(x_t))$). The authors further suggest that input-dependent, non-diagonal transition matrices can overcome this limitation and can simulate *deterministic finite-state automata* (DFAs). [Grazzi et al. \(2024\)](#) extend this result, demonstrating that SSMs whose transition matrices $\mathbf{A}(x_t)$ have only positive eigenvalues (typical in Mamba and Gated DeltaNet) cannot even solve simple state tracking problems like parity. [Grazzi et al. \(2024\)](#) evaluate Mamba-1 ([Gu and Dao, 2024](#)) and Gated DeltaNet ([Yang et al., 2024a](#)) on S_3 and S_5 permutation groups. They demonstrate that Mamba-1 and Gated DeltaNet can solve the tasks when the eigenvalues of \mathbf{A} are allowed to be negative (specifically between $[-1, 1]$). [Siems et al. \(2025\)](#) further demonstrate that allowing a product of $k - 1$ Householder matrices further increases the expressivity and allows solving tasks like S_k . [Terzić et al. \(2025\)](#) take an alternative approach via structured sparse matrices combined with straight-through gradient estimators, which preserves compatibility with parallel scan ([Hillis and Steele, 1986](#); [Blelloch, 1990](#)) while improving expressivity.

2.3.2 Poor in-context retrieval performance

Linear RNNs and SSMS significantly underperform parameter-matched Transformer (Vaswani et al., 2017) models on in-context retrieval tasks (Yang et al., 2023, 2024b,a). While recent linear RNNs such as DeltaNet (Yang et al., 2024b) and Gated DeltaNet (Yang et al., 2024a) have closed this performance gap, there still remains a significant gap between Transformers (Vaswani et al., 2017) and linear RNNs. We experimentally demonstrate this further in Section 5.4.2 (Tables 3, 4).

2.4 Non-Linear RNNs

The most basic non-linear RNN (Elman, 1990) takes the form:

$$h_t = \tanh(\mathbf{W}h_{t-1} + x_t) \quad (8)$$

$$y_t = h_t \quad (9)$$

where $h_t \in \mathbb{R}^{d \times 1}$ is the hidden state at time step t , $x_t \in \mathbb{R}^{d \times 1}$ is the input, and $\mathbf{W} \in \mathbb{R}^{d \times d}$ is the (dense, input-independent) transition matrix.

A key challenge for deep non-linear RNNs is vanishing and exploding gradients, which makes learning long-range dependencies difficult (Bengio et al., 1994). The Long Short-Term Memory (LSTM) (Hochreiter and Schmidhuber, 1997) and Gated Recurrent Unit (GRU) (Cho et al., 2014b) address this by introducing multiplicative gating mechanisms.

Expressivity. Merrill (2019) analyze non-linear RNNs under finite precision and show that they are equivalent to finite-state automata, capable of recognizing all regular languages. Under infinite precision, saturated non-linear RNNs are strictly more expressive, capable of simulating arbitrary deterministic finite-state automata (DFAs) and thus solving hard state-tracking tasks such as permutation group composition that lie outside \mathbf{TC}^0 (Merrill et al., 2024). This expressivity advantage over linear RNNs (which are confined to \mathbf{TC}^0 under diagonal or input-independent transitions) motivates their use in architectures targeting tasks that require stateful computation beyond what Transformers can express.

2.5 Limitations of Non-Linear RNNs

2.5.1 Poor language modeling performance

Despite their expressivity advantages, non-linear RNNs like LSTMs (Hochreiter and Schmidhuber, 1997) and GRUs (Cho et al., 2014a) significantly underperform both Transformers (Vaswani et al., 2017) and modern linear RNNs on language modeling benchmarks. A natural hypothesis is that non-linearity itself is the bottleneck, but we argue the gap is largely attributable to state size. Vector-valued non-linear RNNs maintain a hidden state $h_t \in \mathbb{R}^d$, which is far smaller than the matrix-valued states $\mathbf{H}_t \in \mathbb{R}^{K \times V}$ used by linear attention models (Section 5.6) for the same number of model parameters. Naively increasing d to match this capacity is impractical: the transition matrix $\mathbf{W} \in \mathbb{R}^{d \times d}$ grows quadratically in parameters, and for large d it can no longer fit in the shared memory of a single streaming multiprocessor (SM), eliminating the possibility of on-chip reuse.

2.5.2 Poor in-context retrieval performance

Beyond language modeling, non-linear RNNs also struggle at in-context retrieval tasks. The fundamental bottleneck is again the state size: a vector-valued hidden state $h_t \in \mathbb{R}^d$ must compress the entire context into a fixed-size representation. As sequence length grows, the state becomes increasingly overloaded, making it difficult to retrieve specific key-value associations stored earlier in the context. This stands in contrast to Transformers, which retain all past tokens in an explicit key-value cache and can attend directly to any position. While linear RNNs with matrix-valued states fare better on retrieval due to their larger effective state capacity, they too lag behind Transformers on in-context retrieval and recall-intensive benchmarks (Yang et al., 2023, 2024b,a) (Section 5.4.2). Non-linear RNNs, constrained to vector-valued states, exhibit an even larger retrieval deficit.

2.5.3 Training Inefficiency

Non-Parallelizability on Sequence Length. The element-wise non-linearity in non-linear RNNs breaks the associativity required by the parallel scan algorithm (Hillis and Steele, 1986; Blleloch, 1990), forcing sequential computation over the sequence length. Danieli et al. (2025) show that non-linear RNNs can be parallelized by casting the recurrence as a system of L (L denotes the sequence length) non-linear equations and solving it via Newton’s method (Ortega and Rheinboldt, 2000). However, storing the Jacobian requires substantial memory and the recurrence becomes computationally expensive, rendering the approach impractical at scale. To make it feasible, Danieli et al. (2025) impose diagonal structure on the transition matrix, which eliminates cross-neuron mixing and substantially reduces expressivity. Moreover, each forward pass requires multiple Newton iterations, and the number of iterations needed for convergence is not known a priori for a given architecture. Consequently, executing the full sequential recurrence may ultimately be more efficient than iterative Newton updates.

Expensive Computation due to Back-to-back GEMM for Non-Linear RNNs. Computing the GEMM (General Matrix Multiply) $\mathbf{W}h_{t-1}$ on a GPU proceeds by tiling the output so that each output tile is assigned to a different streaming multiprocessor (SM). This works well for a single GEMM, as each SM can independently compute its tile without cross-SM communication. However, the tiling becomes problematic at the next time step when computing $\mathbf{W}h_t$: the output tiles from time step $t - 1$ become the input tiles for time step t , but they reside on different SMs than where they are needed. Ideally, the SM that produced a given output tile would reuse it directly as input, but the standard tiling prevents this. As a result, intermediate results must be written to and reloaded from global memory (HBM), introducing costly synchronization and data movement. This issue is similar to what one would encounter when fusing two back-to-back GEMMs for MLP computation.

To address this, FlashRNN (Pöppel et al., 2025) modify the RNN recurrence into a block-wise form, analogous to multi-head attention. This design is also adopted by xLSTM (Beck et al., 2024). By keeping the per-block state size small enough to reside in SM shared memory, they avoid HBM-level synchronization and achieve significant speedups.

Poor Hardware Utilization due to Wasted FLOPs. FlashRNN (Pöppel et al., 2025) propose to parallelize a vector-valued non-linear recurrence over the batch dimension (B) and the number of heads (N). However, to enable the use of tensor cores on NVIDIA GPUs, Pöppel et al. (2025) propose to pad the batch dimension B to B_{padded} (16 for using the WMMA instruction) (NVIDIA Corporation). This leads to a GEMM computation with shape $\mathbf{M}, \mathbf{N}, \mathbf{K} = B_{\text{padded}}, d, d$ at each time step.

In practice, per-GPU batch sizes of 16 or more are rarely feasible when training large models due to GPU memory limitations (80GB on NVIDIA H100s), leading to substantial wasted FLOPs due to padding. For example, at a batch size of $B = 4$, padding wastes 75% of the recurrence FLOPs. In Section 3.4, we describe how the M^2 RNN recurrence completely avoids the FLOPs wasted due to padding.

3 Matrix-to-Matrix RNN

In this section, we describe Matrix-to-Matrix RNN (M^2 RNN), our proposed non-linear RNN layer which addresses the poor language modeling, poor retrieval performance and poor hardware utilization of vector-valued non-linear RNNs while also addressing the limited state tracking problem of linear RNNs.

3.1 M^2 RNN Layer

To overcome the state size limitations of traditional RNNs, we develop Matrix-to-Matrix RNN (M^2 RNN), which uses matrix-valued hidden states. We adopt an outer product state expansion strategy similar to that of linear attention (Katharopoulos et al., 2020) and SSMs (Gu and Dao, 2024; Dao and Gu, 2024), significantly increasing the state size without significantly increasing the number of parameters. We further incorporate a forget gate which is independent of the recurrent state and can be computed in parallel. We found that adding a residual connection around the M^2 RNN recurrence similar to SSMs helps to improve gradient flow

and mitigate the compounding effect of the tanh activation across layers. The forward computation for M²RNN recurrence is:

$$\mathbf{Z}_t = \tanh(\mathbf{H}_{t-1}\mathbf{W} + k_t v_t^\top) \quad (10)$$

$$\mathbf{H}_t = f_t \mathbf{H}_{t-1} + (1 - f_t) \mathbf{Z}_t \quad (11)$$

$$y_t = \mathbf{H}_t^\top q_t + w_r \odot v_t \quad (12)$$

where $\mathbf{H}_{t-1} \in \mathbb{R}^{K \times V}$ denotes the recurrent state at the previous time step. We initialize the initial state $\mathbf{H}_0 = 0_{K \times V}$ (matrix of shape $K \times V$ filled with 0s). $\mathbf{Z}_t \in \mathbb{R}^{K \times V}$ denotes the state update and \mathbf{H}_t denotes the state at the current time step after the update. $\mathbf{W} \in \mathbb{R}^{V \times V}$ is the transition matrix for the recurrence (independent of the input) while the query, key, value and forget gate ($q_t, k_t \in \mathbb{R}^{K \times 1}, v_t \in \mathbb{R}^{V \times 1}, f_t \in [0, 1]$) are functions of the input $x_t \in \mathbb{R}^{d \times 1}$. $y_t \in \mathbb{R}^{V \times 1}$ represents the final output of the recurrence after the query readout and residual addition and w_r represents the weight for the residual.

3.1.1 Forget Gate

Following LSTMs (Hochreiter and Schmidhuber, 1997) and GRUs (Cho et al., 2014a), we augment M²RNN with a forget gate to mitigate the vanishing gradient problem. We use a scalar-valued (per-head) forget gate $f_t \in [0, 1]$. While we experimented with a vector-valued forget gate of size K per head, it yielded only marginal improvements while substantially increasing the parameter count. The gated recurrent update is $\mathbf{H}_t = f_t \mathbf{H}_{t-1} + (1 - f_t) \mathbf{Z}_t$, where $f_t = 1$ fully preserves the current state and $f_t = 0$ resets it entirely. Although the importance of forget gates is well established in the literature (Hochreiter and Schmidhuber, 1997; Cho et al., 2014a; Chung et al., 2014), we provide confirmatory ablations in Section 5.6. Note that the forget gate (f_t) is only a function of the input x_t and is independent of the previous state \mathbf{H}_{t-1} unlike LSTMs (Hochreiter and Schmidhuber, 1997) and GRUs (Cho et al., 2014a). The forget gate ($f_{t,n}$)² (forget gate value for n^{th} head at time step t) for M²RNN layers is computed as:

$$f_{t,n} = \psi(x_t) = \frac{1}{(1 + e^{x_t + \beta_n})^{\alpha_n}} \quad (13)$$

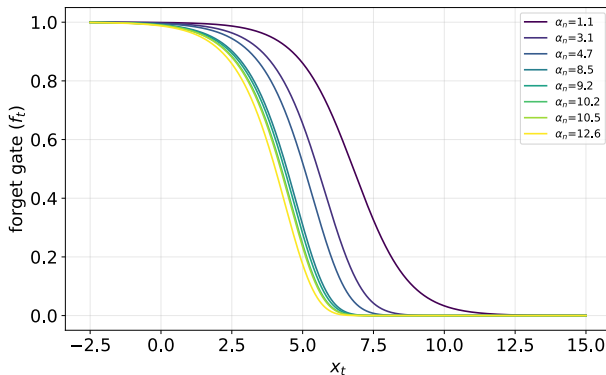


Figure 1 Forget gate (f_t) behavior as a function of the input (x_t) for different values of α_n and β_n . n denotes the n^{th} head.

where α_n and β_n are learnable parameters that are independent of the input. They are initialized to different values for different heads. A smaller value of α_n for the n^{th} head results in a slower decay rate. The parameter β_n controls the location at which the forget gate saturates (see Figure 1). A similar gate is used in Mamba-1 (Gu and Dao, 2024), Mamba-2 (Dao and Gu, 2024) and Gated DeltaNet (Yang et al., 2024a). Each head is initialized to a different value of α_n and β_n which leads to different forgetting characteristics. We initialize $\alpha_n \sim \text{Uniform}(\alpha_{\min}, \alpha_{\max})$ and $\beta_n \sim \text{LogUniform}(\beta_{\min}, \beta_{\max})$. Note that when $\alpha_n = 1$, the forget gate simplifies to $\psi(x_t) = \sigma(-x_t - \beta_n)$ which corresponds to a sigmoid with a reflected input and a bias shift.

²We drop the notation for head $f_{t,n}$ in the rest of the paper and use f_t for simplicity.

3.1.2 M²RNN Block

The queries, keys, and values (q_t, k_t, v_t) are computed via linear projections followed by a depthwise causal short-convolution (kernel size 4) and SiLU activation (Hendrycks, 2016; Elfwing et al., 2018). The output gate g_t uses SiLU without a convolution, and the forget gate f_t uses the parameterized function from Section 3.1.1 to ensure $f_t \in [0, 1]$. Crucially, all pre-recurrence projections depend only on the input x_t and can therefore be computed in parallel across the sequence. The full M²RNN layer (for a single head) is:

$$q_t = \text{SiLU}(\text{conv1d}(\mathbf{W}_q x_t + b_q)) \in \mathbb{R}^{K \times 1} \quad (14)$$

$$k_t = \text{SiLU}(\text{conv1d}(\mathbf{W}_k x_t + b_k)) \in \mathbb{R}^{K \times 1} \quad (15)$$

$$v_t = \text{SiLU}(\text{conv1d}(\mathbf{W}_v x_t + b_v)) \in \mathbb{R}^{V \times 1} \quad (16)$$

$$f_t = \psi(\mathbf{W}_f x_t) \in [0, 1] \quad (17)$$

$$g_t = \text{SiLU}(\mathbf{W}_g x_t) \in \mathbb{R}^{V \times 1} \quad (18)$$

$$\mathbf{Z}_t = \tanh(\mathbf{H}_{t-1} \mathbf{W} + k_t v_t^\top) \in \mathbb{R}^{K \times V} \quad (19)$$

$$\mathbf{H}_t = f_t \mathbf{H}_{t-1} + (1 - f_t) \mathbf{Z}_t \in \mathbb{R}^{K \times V} \quad (20)$$

$$y_t = \mathbf{H}_t^\top q_t + w_r \odot v_t \in \mathbb{R}^{V \times 1} \quad (21)$$

$$y_{gt} = \text{RMSNorm}(y_t \odot g_t) \in \mathbb{R}^{V \times 1} \quad (22)$$

$$o_t = \mathbf{W}_o y_{gt} \in \mathbb{R}^{d \times 1} \quad (23)$$

$$(24)$$

where $x_t \in \mathbb{R}^d$.

Following Mamba-1 (Gu and Dao, 2024), Mamba-2 (Dao and Gu, 2024), and Gated DeltaNet (Yang et al., 2024a), we adopt a hybrid architecture combining the H3 block (Fu et al., 2022) with a gated MLP, a design that has proven effective in production LLMs (Figure 2).

Transition Matrix Initialization. We experimented with three initialization schemes for the transition matrix \mathbf{W} : normal initialization ($\mathbf{W} \sim \mathcal{N}(0, \sigma^2)$), orthogonal initialization ($\mathbf{W}\mathbf{W}^\top = \mathbf{I}$), and identity initialization ($\mathbf{W} = \mathbf{I}$) (Le et al., 2015). Consistent with findings for vector-valued non-linear RNNs, orthogonal initialization outperforms normal initialization. Identity initialization performs on par with orthogonal initialization, so we adopt it for all models.

Gradient Clipping. Training non-linear RNNs with backpropagation through time (BPTT) is susceptible to exploding gradients, as the gradient of the loss with respect to early hidden states involves repeated multiplication by the transition matrix \mathbf{W} and the Jacobian of the tanh nonlinearity. Although the forget gate f_t attenuates gradients flowing through the state, the transition matrix \mathbf{W} can still cause gradient magnitudes to grow unboundedly. To stabilize training, we apply per-step gradient clipping to the gradient of the recurrent state \mathbf{H}_t during BPTT.

3.2 Improved State Tracking

Theorem 1. *The M²RNN recurrence can represent all tasks representable by non-linear vector-valued RNNs and hence can represent regular languages.*

We give the proof for Theorem 1 in Appendix B.

Siems et al. (2025) show that Gated DeltaProduct $[-1, 1]^3$ parameterized as a product of $k - 1$ Householder matrices can, in principle, represent the S_k task. In particular, this implies that the S_3 task should be representable using Gated DeltaProduct $[-1, 1]$ with product of two Householder matrices. To evaluate this claim empirically, we compare M²RNN, GRU (Cho et al., 2014a), Gated DeltaNet $[-1, 1]^4$ (Yang et al.,

³Gated DeltaProduct $[-1, 1]$ denotes Gated DeltaProduct with the ability to have negative eigenvalues.

⁴Gated DeltaNet $[-1, 1]$ denotes Gated DeltaNet with the ability to have negative eigenvalues.

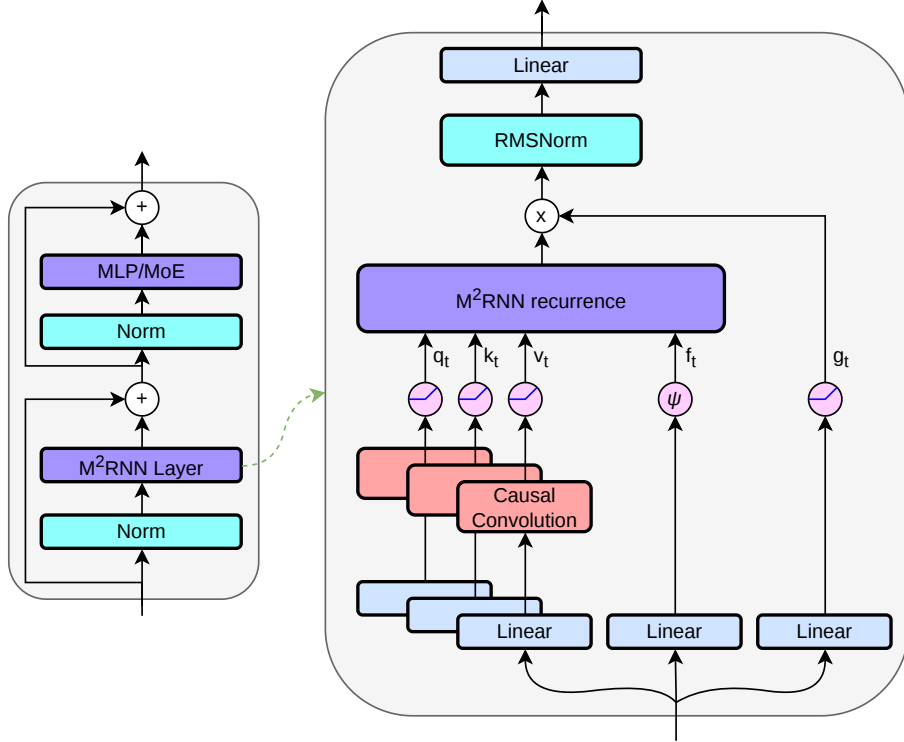


Figure 2 Visualization of the Matrix-to-Matrix RNN layer. This block replaces attention and is combined with MLP and RMSNorm modules as in the Transformer.

2024a), and Gated DeltaProduct $[-1, 1]$ (Siems et al., 2025) parameterized as a product of two Householder matrices on the S_3 task. All models are trained on sequences of length 128 and evaluated on context lengths up to 512.

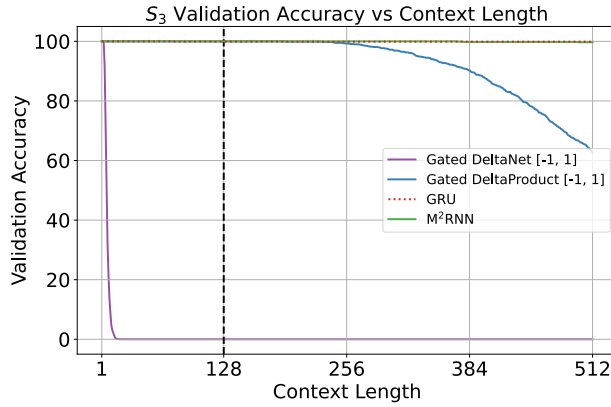


Figure 3 Accuracy on the permutation group S_3 state-tracking task for M^2RNN , Gated DeltaNet $[-1, 1]$, Gated DeltaProduct $[-1, 1]$ and GRU. The vertical line at 128 denotes the training context length for all models. For the Gated DeltaProduct, we use product of 2 HouseHolder matrices since it can solve the S_3 task in theory (Grazzi et al., 2024). However, as the evaluation context length is increased beyond the training context length, we observe accuracy degradation.

As can be seen from Figure 3, Gated DeltaNet $[-1, 1]$ fails to learn the task altogether. Gated DeltaProduct $[-1, 1]$ achieves near-perfect accuracy up to context length 256, however, it fails to generalize to longer

sequence lengths not seen during training. These findings suggest that, despite its theoretical expressivity, the model exhibits limited length generalization even on the simple state-tracking S_3 task. However, both GRU (Cho et al., 2014a) and M²RNN generalize perfectly to unseen context lengths achieving $\geq 99.5\%$ accuracy up to 512 sequence length. This suggests that theoretical expressivity alone does not guarantee robust state tracking in practice, and that non-linear RNNs like M²RNN and GRU exhibit stronger length generalization on this task. Motivated by this, we investigate whether non-linear RNNs exhibit this length generalization advantage on language modeling when equipped with an expanded state size.

3.3 Improved Language Modeling, In-Context Retrieval and Long-Context Performance

The outer-product formulation for state size expansion for RNNs has become standard in many SSMs and linear RNNs (Yang et al., 2023; Gu and Dao, 2024; Dao and Gu, 2024; Yang et al., 2024b,a). Qin et al. (2024) demonstrate that larger state sizes improve language modeling performance even when achieved through low-rank parameterizations. We also demonstrate this with empirical evidence in Section 5.6.

Additionally, Mamba-2 (Dao and Gu, 2024) increases the effective state size through a grouping strategy that shares parameters across heads using a multi-value attention formulation, allowing the model to scale the state dimension without increasing the overall parameter count. Building on this idea, we use an outer product with the multi-value attention formulation proposed by Dao and Gu (2024) to increase the achievable state size under a fixed parameter budget (see Table 8 in Appendix A).

The expanded matrix-valued state directly addresses the two core weaknesses of vector-valued non-linear RNNs identified in Section 2.5: poor language modeling and poor retrieval performance.

Language modeling. The low language modeling performance of non-linear RNNs such as LSTMs (Hochreiter and Schmidhuber, 1997) and GRUs (Cho et al., 2014a) relative to Transformers (Vaswani et al., 2017) and linear RNNs has traditionally been attributed to the non-linearity itself. We argue instead that the primary bottleneck is state capacity. By expanding the hidden state from a vector $h_t \in \mathbb{R}^d$ to a matrix $\mathbf{H}_t \in \mathbb{R}^{K \times V}$, M²RNN dramatically increases the information that can be stored at each recurrent step without a proportional increase in parameter count. We provide empirical evidence for this in Section 5.6, showing that larger state sizes yield consistent language modeling improvements under a fixed parameter budget.

In-context retrieval and long-context performance. The outer product write $k_t v_t^\top$ significantly expands the state size enabling efficient storage of key-value associations and structured in-context retrieval via the readout $\mathbf{H}_t^\top q_t$. This capacity is absent in vector-valued non-linear RNNs, which cannot store enough associations due to the limited state size. We demonstrate the resulting gains in Tables 3, 4. We further demonstrate the impact of the state size expansion in long-context tasks in Tables 5, 6.

3.4 Improved Hardware Utilization

3.4.1 Improved Tiling

The outer product expansion enables M²RNN to be efficiently parallelized across both the batch dimension B and the number of heads N . In this formulation, each GPU streaming multiprocessor (SM) executes an independent recurrence over a matrix-valued state of size $K \times V$. Each step of the recurrence involves a GEMM with dimensions $\mathbf{M}, \mathbf{N}, \mathbf{K} = K, V, V$.

Importantly, the matrix-valued recurrence in M²RNN requires no padding as long as K and V are multiples of 16 allowing utilizing the tensor cores. For example, when $K = 64$ and $V = 16$, the GEMM computation $\mathbf{H}_{t-1} \mathbf{W}$ can utilize the WGMMMA instruction on NVIDIA Hopper GPUs (NVIDIA Corporation), ensuring high hardware efficiency.

Crucially, the GEMM shape in M²RNN is independent of the batch size B . This contrasts with vector-valued non-linear RNNs, where GEMM dimensions depend on B , often necessitating batch-size padding to achieve tensor core compatibility. As a result, the outer product state expansion mechanism achieves improved parallelism without wasting FLOPs, avoiding the padding overhead described in Section 2.5.3.

3.4.2 Efficient Integration of M²RNN Layers in Hybrid Architectures

Due to the expensive nature of M²RNN layers, we explore using them more sparingly. Our results show that replacing only a single Mamba-2 or Gated DeltaNet layer with M²RNN in a hybrid architecture achieves the same accuracy improvements as the full hybrid M²RNN model, while keeping training throughput within 6% of the Hybrid Gated DeltaNet at both 4k and 16k context lengths. This provides a scalable strategy for incorporating M²RNN layers into large language models.

4 Distributed Training and Systems Optimizations

In this section, we discuss the system considerations for M²RNN layers, including the forward and backward algorithms (Section 4.1, 4.2) and tensor parallelism (Section 4.3).

Algorithm 1 Forward Computation for M²RNN layer with multi-value attention formulation. The [blue colour](#) indicates computation or tensors residing in on-chip memory.

```

input :  $\mathbf{H}_0 \in \mathbb{R}^{BNKV}$ ,  $\mathbf{Q}, \mathbf{K} \in \mathbb{R}^{BTK}$ ,  $\mathbf{V} \in \mathbb{R}^{BTV}$ ,  $\mathbf{W} \in \mathbb{R}^{NVV}$ ,  $\mathbf{F} \in [0, 1]^{BTN}$ 
output :  $\mathbf{Y} \in \mathbb{R}^{BTV}$ 
  for  $n = 0$  to  $N - 1$  in parallel do  $\triangleright$  Each head on a separate SM
    Load  $\mathbf{W} \leftarrow \mathbf{W}[n, :, :]$  from HBM  $\triangleright$  Transition matrix to SRAM (reused across batch)
    for  $b = 0$  to  $B - 1$  in parallel do
      Load  $\mathbf{H} \leftarrow \mathbf{H}_0[b, n, :, :]$  from HBM  $\triangleright$  Initial hidden state ( $K \times V$ ) to SRAM
      for  $t = 0$  to  $T - 1$  do  $\triangleright$  Sequential recurrence over time
        Load  $q, k, v, f \leftarrow \mathbf{Q}[b, t, :], \mathbf{K}[b, t, :], \mathbf{V}[b, t, n, :], \mathbf{F}[b, t, n]$  from HBM
        Compute  $\mathbf{Z} \leftarrow \tanh(\mathbf{HW} + kv^\top)$   $\triangleright$  Nonlinear transition with outer product input
        Compute  $\mathbf{H} \leftarrow f\mathbf{H} + (1 - f)\mathbf{Z}$   $\triangleright$  Gated update of hidden state
        Compute  $y \leftarrow \mathbf{H}^\top q$   $\triangleright$  Query readout from hidden state
        Store  $\mathbf{Y}[b, t, n, :] \leftarrow y$  to HBM  $\triangleright$  Write output; no intermediate  $\mathbf{H}$  cached
      end for
    end for
  end for

```

4.1 Forward Algorithm

We implement the forward computation for the M²RNN layer using the Triton (Tillet et al., 2019) DSL. The kernel parallelizes across the batch dimension B and the number of heads N , assigning each (b, n) pair to a separate GPU SM. We illustrate our algorithm in Algorithm 1 for the case of multi-value formulation ($N_q = N_k = 1$ and $N_v, N_f, N_w = N$) which we use for all our models. We avoid caching intermediate activations during the backward pass for use in backward computation since storing the \mathbf{H} matrix is prohibitively expensive in both IO and the memory footprint, since $\mathbf{H}_t \in \mathbb{R}^{BNKV}$ is much larger than the per time step keys and values ($k_t \in \mathbb{R}^{N_k K}$, $v_t \in \mathbb{R}^{N_v V}$).

4.2 Backward Algorithm

For the backward computation, we recompute the forward recurrence without the final query readout and cache \mathbf{H}_t at every time step to HBM. The backward kernel then reads \mathbf{H}_t at every time step from HBM to compute the gradients for the inputs. The backward kernel is implemented in the Triton DSL (Tillet et al., 2019), which does not expose direct programmability of shared memory. As a result, the kernel is heavily memory-bandwidth bound. We are developing an optimized implementation in CUTLASS to address this bottleneck. The algorithm is illustrated in Algorithm 2.

4.3 Tensor Parallelism

Shoeybi et al. (2019) introduced tensor parallelism (TP), a model parallelism technique that partitions attention and MLP layers across multiple accelerators. This approach has become standard for training large-

Algorithm 2 Backward Computation for M²RNN layer with multi-value attention formulation. The **blue colour** indicates computation or tensors residing in on-chip memory.

input : $\mathbf{H}_0 \in \mathbb{R}^{BNKV}$, $\mathbf{Q} \in \mathbb{R}^{BTK}$, $\mathbf{K} \in \mathbb{R}^{BTK}$, $\mathbf{V} \in \mathbb{R}^{BTNV}$, $\mathbf{W} \in \mathbb{R}^{NVV}$, $\mathbf{F} \in [0, 1]^{BTN}$, $\mathbf{H}_{\text{full}} \in \mathbb{R}^{BTNKV}$
output : $d\mathbf{Q} \in \mathbb{R}^{BTK}$, $d\mathbf{K} \in \mathbb{R}^{BTK}$, $d\mathbf{V} \in \mathbb{R}^{BTNV}$, $d\mathbf{W} \in \mathbb{R}^{NVV}$, $d\mathbf{F} \in [0, 1]^{BTN}$

```

for  $n = 0$  to  $N - 1$  in parallel do ▷ Each head on a separate SM
  Load  $\mathbf{W} \leftarrow \mathbf{W}[n, :, :]$  from HBM ▷ Transition matrix to SRAM
  for  $b = 0$  to  $B - 1$  in parallel do
    Load  $\mathbf{H} \leftarrow \mathbf{H}_0[b, n, :, :]$  from HBM ▷ Initial hidden state to SRAM
    for  $t = 0$  to  $T - 1$  do ▷ Pass 1: forward recomputation, cache all  $\mathbf{H}_t$ 
      Load  $k, v, f \leftarrow \mathbf{K}[b, t, :], \mathbf{V}[b, t, n, :], \mathbf{F}[b, t, n]$  from HBM
      Store  $\mathbf{H}_{\text{full}}[b, t, n, :, :] \leftarrow f\mathbf{H} + (1 - f) \tanh(\mathbf{H}\mathbf{W} + kv^\top)$  to HBM ▷ Cache hidden state for backward
    end for
     $d\mathbf{W} \leftarrow 0_{V \times V}$  ▷ Initialize  $d\mathbf{W}$  to 0
    for  $t = T - 1$  to  $0$  do ▷ Pass 2: reverse sweep to compute gradients
      if  $t == 0$  then
        Load  $\mathbf{H}_{\text{prev}} \leftarrow \mathbf{H}_0[b, n, :, :]$  from HBM
      else
        Load  $\mathbf{H}_{\text{prev}} \leftarrow \mathbf{H}_{\text{full}}[b, t - 1, n, :, :]$  from HBM
      end if
      Load  $q, k, v, f, dy \leftarrow \mathbf{Q}[b, t, :], \mathbf{K}[b, t, :], \mathbf{V}[b, t, n, :], \mathbf{F}[b, t, n], d\mathbf{Y}[b, t, n, :]$  from HBM
      Compute  $\mathbf{Z} \leftarrow \tanh(\mathbf{H}_{\text{prev}}\mathbf{W} + kv^\top)$  ▷ Recompute pre-gate activation
      Compute  $\mathbf{H} \leftarrow f\mathbf{H}_{\text{prev}} + (1 - f)\mathbf{Z}$  ▷ Recompute hidden state at  $t$ 
      Compute  $dq \leftarrow \mathbf{H} \cdot dy$  ▷ Gradient w.r.t. query
      Atomic Add  $d\mathbf{Q}[b, t, :] \leftarrow dq$  to HBM ▷ Accumulate across shared heads
      Compute  $r \leftarrow q \cdot dy^\top$  ▷ Outer product for temporary variable
      Compute  $df \leftarrow \frac{1}{K} [r \odot (\mathbf{H}_{\text{prev}} - \mathbf{Z})] 1_V$  ▷ Gradient w.r.t. forget gate (scalar)
      Store  $d\mathbf{F}[b, t, n] \leftarrow df$  to HBM
      Compute  $d\mathbf{H} \leftarrow r \odot f$  ▷ Gradient through the gated residual
      Compute  $d\mathbf{Z} \leftarrow r \odot (1 - f)$  ▷ Gradient through the nonlinear branch
      Compute  $d\mathbf{X} \leftarrow d\mathbf{Z} \odot (\mathbf{1}_{K \times V} - \mathbf{Z} \odot \mathbf{Z})$  ▷ Backprop through tanh
      Compute  $d\mathbf{H} \leftarrow d\mathbf{Z} \odot (d\mathbf{X} \cdot \mathbf{W}^\top)$  ▷ Gradient w.r.t. previous hidden state
      Compute  $d\mathbf{W} \leftarrow d\mathbf{W} + \mathbf{H}_{\text{prev}}^\top d\mathbf{X}$  ▷ Accumulate gradient for transition matrix
      Compute  $dk \leftarrow d\mathbf{X} \cdot v$  ▷ Gradient w.r.t. key
      Atomic Add  $d\mathbf{K}[b, t, :] \leftarrow dk$  to HBM ▷ Accumulate across shared heads
      Compute  $dv \leftarrow d\mathbf{X}^\top k$  ▷ Gradient w.r.t. value
      Store  $d\mathbf{V}[b, t, n, :] \leftarrow dv$  to HBM ▷ Write to HBM
    end for
    Atomic Add  $d\mathbf{W}[n, :, :] \leftarrow d\mathbf{W}$  to HBM ▷ Accumulate  $d\mathbf{W}$  across batch
  end for
end for

```

scale models (Chowdhery et al., 2023; Smith et al., 2022; Grattafiori et al., 2024; Brown et al., 2020; Workshop et al., 2022). The core challenge in applying TP for M²RNN is that the multi-value formulation shares a single query and key head across all value heads ($N_q = N_k = 1$, $N_v = N$), preventing a straightforward partition of heads across GPUs. We present two strategies for implementing TP in M²RNN layers: a grouped-value approach that avoids extra communication, and a multi-value approach that preserves the parameter count at the cost of additional communication during training. We represent the TP world size as N_{TP} .

4.3.1 TP Topology-Aware M²RNN Layers

A straightforward way to implement TP for M²RNN layers is to adopt a grouped-value formulation: the number of query and key heads is set equal to the TP world size ($N_q = N_k = N_{\text{TP}}$), while the number of

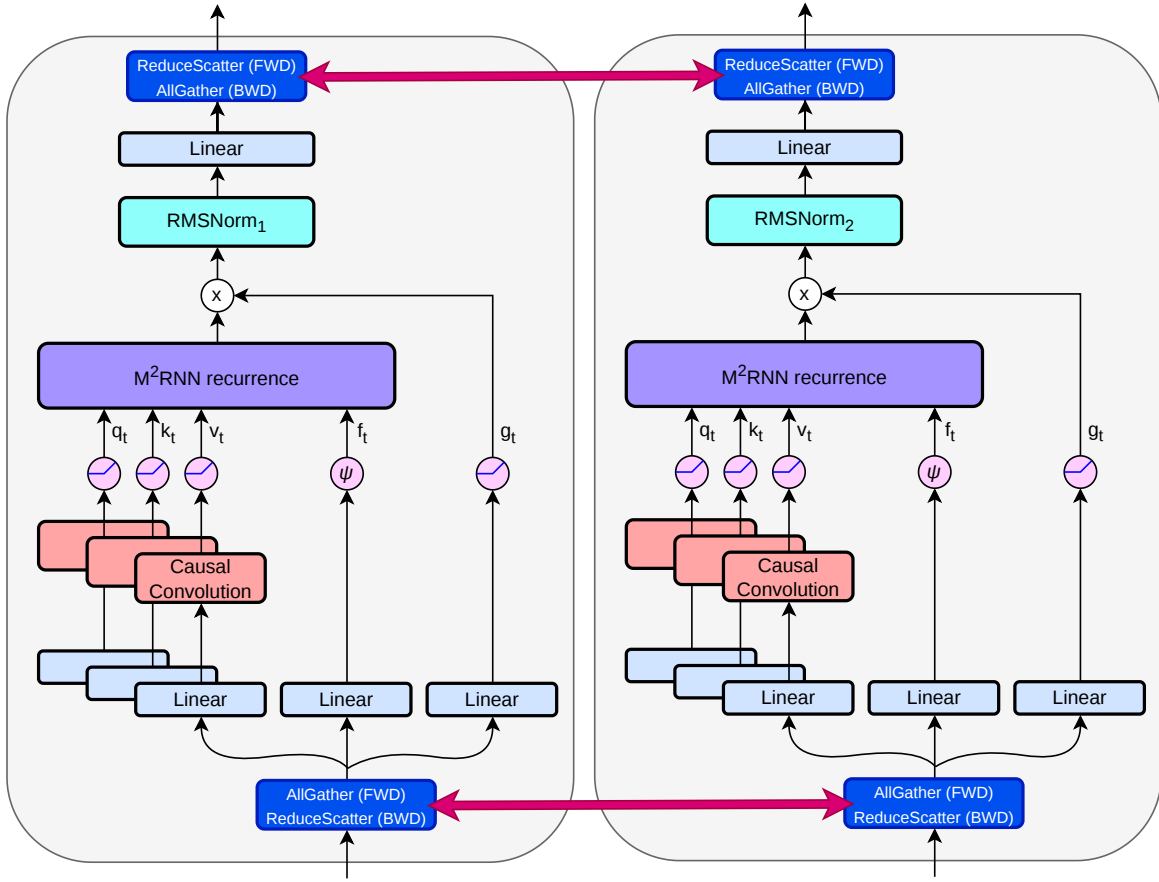


Figure 4 TP topology-aware M^2RNN layer running with TP on 2 GPUs. Note that $RMSNorm_1$ and $RMSNorm_2$ have different weights for the RMSNorm module on both GPUs.

value heads remains $N_v = N$. Each GPU is assigned one query head, one key head, and $\frac{N_v}{N_{TP}}$ value heads⁵, and applies RMSNorm (Zhang and Sennrich, 2019) with different weights on different GPUs in the TP group (refer to Figure 4). Since this is equivalent to running a multi-value M^2RNN recurrence on every GPU, this requires no modifications to the kernels.

Advantages. Each GPU operates independently on its assigned heads, so no communication is introduced beyond the standard TP communication required for an attention layer.

Disadvantages. The query and key projection sizes grow proportionally with N_{TP} , coupling the parameter count to the TP topology used during training⁶. Consequently, a model trained with TP world size N_{TP} cannot be straightforwardly deployed at a smaller world size without carrying the inflated query, key projections and the larger activation footprint that comes with them (specifically, the input to the output linear projection). This is analogous to the approach proposed in Mamba-2 (Dao and Gu, 2024) and the Desync-Residual strategy⁷ (Zhang et al., 2025).

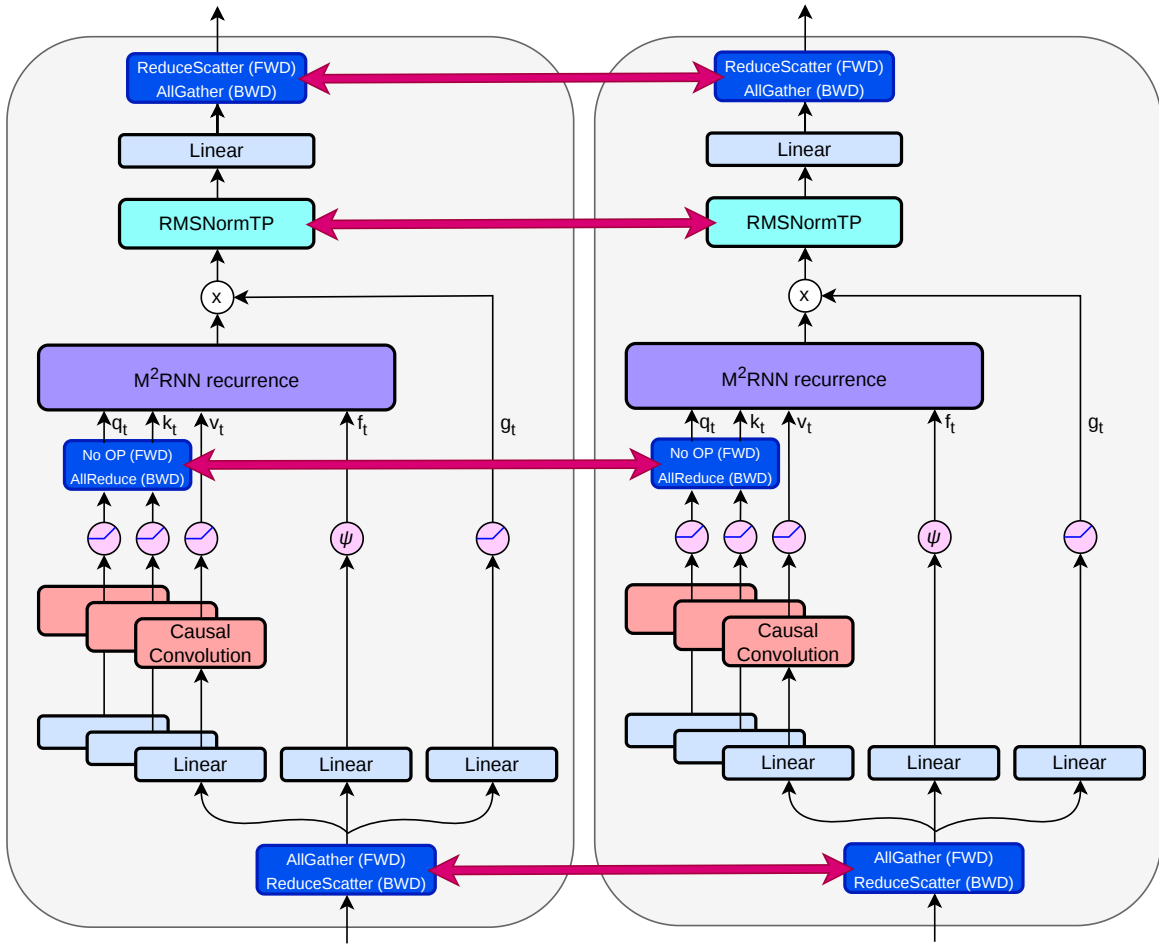


Figure 5 TP topology-independent M^2RNN layer. Note that RMSNormTP have weights sharded along the model width dimension for the RMSNorm module on both GPUs requiring a synchronization in both the forward and backward computation.

4.3.2 TP Topology-Independent M^2RNN Layers

Alternatively, TP can be applied directly to the multi-value formulation ($N_q = N_k = 1, N_v = N$). Each GPU processes $\frac{N}{N_{TP}}$ value heads but shares the same query and key projections. This requires replacing RMSNorm (Zhang and Sennrich, 2019) modules with RMSNormTP (refer to Appendix C) where the weight for RMSNorm is sharded and an extra communication is introduced in RMSNormTP for the forward and backward computation. The communication in the forward is required to synchronize the RMSNorm normalization term and the synchronization in the backward is required for computing the activation gradient. Note that this idea is applicable to Mamba-2 (Dao and Gu, 2024) and Gated DeltaNet (Yang et al., 2024a) layers as well. If the weights for the causal-convolution and linear projections for queries and keys are initialized to the same values on all GPUs participating in TP, the sharding method illustrated in Figure 5 ensures that the weights remain synchronized during training.

Advantages. This TP approach preserves the parameter count regardless of the number of GPUs and makes the M^2RNN layers independent of the TP topology used during training.

⁵We assume N_v is divisible by N_{TP} .

⁶The RMSNorm weight size also grows with N_{TP} but is significantly smaller in comparison.

⁷Refer to <https://arxiv.org/abs/2501.06589v2> (v2) since later versions of the paper dropped Desync-Residual.

Disadvantages. This approach introduces additional AllReduce communications beyond standard TP. In the forward pass, one extra AllReduce is needed to synchronize the RMSNorm normalization term⁸. The backward pass requires three extra AllReduces: one for the RMSNorm gradient and two to aggregate the query and key activation gradients, since each GPU computes partial gradients for the shared query and key heads from its assigned subset of value heads. Weight gradients for the query and key projections remain naturally synchronized across GPUs throughout training, provided the corresponding weights are initialized identically, so no additional communication is needed for them. One way to reduce backward communication is to make only the RMSNorm module TP topology-dependent (as in Section 4.3.1); since RMSNorm has very few parameters, this trade-off may be acceptable in practice.

5 Experiments

We train dense models with 410M parameters (24 layers) and Mixture-of-Experts (MoE) (Shazeer et al., 2017) models with 7B total (1.1B active) parameters (40 layers). All models are trained on 100B tokens sampled from the high quality subset of Nemotron-CC-v2 (NVIDIA et al., 2025).

5.1 Models

5.1.1 Homogeneous Architectures

We compare M²RNN primarily against Mamba-2 (Dao and Gu, 2024), Gated DeltaNet (Yang et al., 2024a), RNN and GRU (Cho et al., 2014a). We focus on Mamba-2 and Gated DeltaNet because they (and their variants) have demonstrated strong performance in state-of-the-art production models (Team et al., 2025; NVIDIA et al., 2025; Lieber et al., 2024; IBM Granite Team, 2025).

5.1.2 2-way Hybrid Models

We additionally run experiments in hybrid settings that combine recurrent layers with attention layers. Following common practice in production LLMs (IBM Granite Team, 2025; Lieber et al., 2024), we use 1 attention layer for every 7 recurrent layers (i.e., 1 out of every 8 layers is attention). We compare Hybrid M²RNN against Transformer++ (Vaswani et al., 2017), Hybrid Mamba-2 and Hybrid Gated DeltaNet.

5.1.3 3-way Hybrid Models

We also experiment with augmenting Hybrid Gated DeltaNet models with M²RNN layers, yielding 3-way hybrids denoted “Hybrid GDN + M²RNN- n ”, where n is the number of M²RNN layers. For $n = 1$, we replace the first recurrent layer with M²RNN; for $n > 1$, we replace the layer immediately preceding each attention layer, producing “Hybrid GDN + M²RNN-3” and “Hybrid GDN + M²RNN-5” for the 410M and 7B models respectively.

5.2 Model Training

For all the models, we use RMSNorm (Zhang and Sennrich, 2019) with pre-normalization (Xiong et al., 2020). Additionally, Transformer++ uses RoPE positional embeddings (Su et al., 2024) while all linear and hybrid architectures use NoPE (no positional embeddings) (Kazemnejad et al., 2023). For MLP and MoE layers (Shazeer et al., 2017), we use the SwiGLU activation (Shazeer, 2020). We keep the model width, intermediate MLP width, number of layers, and all other hyperparameters consistent across architectures, adjusting only the parameters in the sequence mixing block.

All models are trained with the AdamW optimizer (Loshchilov and Hutter, 2019) using a cosine learning rate schedule. We linearly warm up the learning rate over the first 10B tokens to a peak value of 3×10^{-4} , followed by decaying to 10% of the peak (3×10^{-5}). We use gradient clipping of 1 and weight decay of 0.1. We don’t apply weight decay to the normalization parameters. All models are trained with a batch size of 1024 samples

⁸The RMSNorm normalization term depends only on the batch size (B) and sequence length (T), so this communication is lightweight.

at a context length of 4096 tokens. We ensure that all models see identical data in identical order to ensure fair comparison. The 410M dense models are trained on 32 H100s and the 7B MoE models on 64 H100s.

We use the lm-engine codebase (Mishra, 2024) written in PyTorch (Paszke et al., 2019) for training all our models. We also use FlashAttention-3 (Shah et al., 2024) and SonicMoE (Guo et al., 2025) with PyTorch compile (Ansel et al., 2024) for training throughput optimization. We also use fast kernels for causal convolutions, Mamba-2, Gated DeltaNet, and M²RNN where applicable. The models use mixed precision (Micikevicius et al., 2017) in BF16 (Kalamkar et al., 2019), with gradient AllReduce and accumulation in FP32 for numerical stability.

5.3 Language Modeling

We evaluate all trained models on a suite of downstream benchmarks using EleutherAI’s LM Eval Harness (Gao et al., 2024): LAMBADA (Paperno et al., 2016), HellaSwag (Zellers et al., 2019), PIQA (Bisk et al., 2019), ARC (Clark et al., 2018), Winogrande (Sakaguchi et al., 2019), BoolQ (Clark et al., 2019), OpenBookQA (Mihaylov et al., 2018), CoPA (Roemmele et al., 2011), and SciQ (Welbl et al., 2017). We additionally report language modeling perplexity on Wikitext (Merity et al., 2017) and LAMBADA (Paperno et al., 2016).

Model	Wiki PPL	LMB PPL	LAMBADA	HellaSwag	PIQA	ARC-E	ARC-C	WinoGrande	BoolQ	OBQA	COPA	SciQ	Avg Acc
Mamba-2	22.93	38.56	32.78	47.70	70.29	62.04	30.55	53.28	58.69	33.20	69.00	85.50	<u>54.30</u>
Gated DeltaNet	<u>22.70</u>	34.17	34.21	47.16	71.00	61.24	28.07	51.07	58.84	32.80	70.00	85.50	53.99
RNN	33.74	317.38	13.00	44.12	69.70	62.54	30.63	49.72	45.75	33.40	63.00	77.10	48.90
GRU	25.80	63.83	26.10	48.70	71.49	64.90	30.97	49.64	57.68	33.80	71.00	82.90	53.72
M ² RNN	22.92	<u>33.63</u>	33.98	47.76	71.60	62.29	30.29	53.43	50.21	34.80	72.00	86.00	54.24
Transformer++	23.32	42.87	33.36	45.02	68.88	59.76	29.01	50.43	54.56	32.00	72.00	84.00	52.90
Hybrid Mamba-2	21.59	35.84	35.32	48.11	70.89	62.54	29.35	52.72	51.41	35.40	65.00	86.80	53.75
Hybrid Gated DeltaNet	21.89	<u>29.02</u>	35.78	47.19	70.67	61.91	29.78	52.17	52.57	34.00	70.00	86.30	54.04
Hybrid M ² RNN	<u>21.53</u>	37.31	35.67	48.74	70.29	63.38	30.29	51.46	50.09	33.80	71.00	86.80	<u>54.15</u>
Hybrid Mamba-2	21.59	35.84	35.32	48.11	70.89	62.54	29.35	52.72	51.41	35.40	65.00	86.80	53.75
Hybrid Mamba-2 + M ² RNN-1	21.48	36.98	34.47	48.23	70.46	64.14	31.57	54.46	49.54	33.60	70.00	85.80	<u>54.23</u>
Hybrid Mamba-2 + M ² RNN-3	<u>21.39</u>	<u>35.77</u>	35.77	48.47	70.57	62.33	31.83	50.75	51.44	33.00	65.00	87.40	53.65
Hybrid Gated DeltaNet	21.89	29.02	35.78	47.19	70.67	61.91	29.78	52.17	52.57	34.00	70.00	86.30	54.04
Hybrid Gated DeltaNet + M ² RNN-1	21.39	33.78	34.83	48.11	70.73	61.24	29.95	51.70	48.41	33.20	72.00	87.30	53.75
Hybrid Gated DeltaNet + M ² RNN-3	21.26	28.93	37.18	48.83	69.64	63.85	29.44	53.35	59.14	33.80	71.00	86.10	55.23

Table 1 Language Modeling on the 410M parameter dense model across commonsense reasoning benchmarks. All models are evaluated in the 0-shot setting.

Model	Wiki PPL	LMB PPL	LAMBADA	HellaSwag	PIQA	ARC-E	ARC-C	WinoGrande	BoolQ	OBQA	COPA	SciQ	Avg Acc
Mamba-2	<u>13.73</u>	<u>11.03</u>	50.09	67.43	76.82	74.33	43.52	61.64	64.01	41.00	80.00	93.40	<u>65.22</u>
Gated DeltaNet	13.89	11.10	48.92	66.94	77.26	73.82	40.53	60.14	65.41	39.60	78.00	92.20	64.28
RNN	17.65	43.68	30.25	64.49	76.61	72.64	41.04	55.64	58.35	40.20	79.00	87.60	60.58
GRU	14.80	15.33	43.94	67.36	76.82	75.67	43.52	58.96	63.79	41.00	82.00	91.30	64.44
M ² RNN	13.80	11.48	49.18	67.57	76.71	75.51	44.97	58.17	64.16	41.40	82.00	92.00	65.17
Transformer++	14.94	17.26	43.90	62.99	75.63	71.97	38.91	57.54	63.12	37.20	75.00	91.40	61.76
Hybrid Mamba-2	13.10	11.05	50.18	68.62	76.55	72.64	43.09	60.62	63.61	43.00	79.00	93.00	65.03
Hybrid Gated DeltaNet	13.51	11.06	50.20	67.23	77.09	73.06	41.64	59.12	62.39	40.80	82.00	92.90	64.64
Hybrid M ² RNN	<u>13.00</u>	<u>10.58</u>	51.74	68.44	76.55	76.81	43.09	61.09	63.21	40.40	81.00	93.30	<u>65.56</u>
Hybrid Mamba-2	13.10	11.05	50.18	68.62	76.55	72.64	43.09	60.62	63.61	43.00	79.00	93.00	65.03
Hybrid Mamba-2 + M ² RNN-1	<u>13.01</u>	<u>10.84</u>	50.92	68.35	77.86	74.66	42.24	60.54	62.57	40.40	83.00	92.80	65.33
Hybrid Mamba-2 + M ² RNN-5	13.02	11.59	49.84	68.19	77.04	75.17	42.58	59.04	65.26	42.40	83.00	93.90	<u>65.64</u>
Hybrid Gated DeltaNet	13.51	11.06	50.20	67.23	77.09	73.06	41.64	59.12	62.39	40.80	82.00	92.90	64.64
Hybrid Gated DeltaNet + M ² RNN-1	13.07	10.33	51.54	68.69	78.18	74.45	41.81	60.30	65.08	42.00	82.00	93.90	65.80
Hybrid Gated DeltaNet + M ² RNN-5	12.85	10.29	51.80	68.99	76.82	76.73	43.60	60.69	63.30	40.20	81.00	93.50	65.66

Table 2 Language Modeling on the 7B (1B active) MoE model across commonsense reasoning benchmarks. All models are evaluated in the 0-shot setting.

5.3.1 Homogeneous Architectures

At the 410M scale, Gated DeltaNet achieves the best Wikitext (Merity et al., 2017) perplexity among all baselines, with M²RNN matching Mamba-2 (Dao and Gu, 2024) (within 0.01 points). On LAMBADA (Paperno et al., 2016), M²RNN outperforms both Mamba-2 and Gated DeltaNet (Yang et al., 2024a) by 4.93 and 0.54 perplexity points respectively (Table 1). We attribute M²RNN’s gap behind Gated DeltaNet on Wikitext to its 3× smaller state size: while increasing the state size can close this gap, it also raises the per-step FLOP count of the recurrence, making it a less favorable tradeoff in practice.

At the 7B MoE scale, Mamba-2 achieves the best Wikitext perplexity, followed by M²RNN, which outperforms Gated DeltaNet by 0.09 points (Table 2). On average downstream accuracy, M²RNN matches Mamba-2 to within 0.06 points at both the 410M and 7B MoE scales while consistently outperforming Gated DeltaNet (Tables 1, 2). Vanilla RNN and GRU models significantly underperform M²RNN and other linear RNNs across all metrics.

5.3.2 2-way Hybrid Models

Combining M²RNN with attention (Vaswani et al., 2017) (denoted Hybrid M²RNN) yields substantial gains on Wikitext (Merity et al., 2017). Hybrid M²RNN outperforms Hybrid Mamba-2 (Dao and Gu, 2024) by 0.06 and 0.1 perplexity points at 410M and 7B MoE scale, and Hybrid Gated DeltaNet (Yang et al., 2024a) by 0.4 and 0.5 points at the 410M and 7B MoE scale. Average downstream accuracy also improves over all other hybrids at both scales (Tables 1, 2). Overall, 2-way hybrids improve upon both Transformer++ and homogeneous M²RNN models. We attribute these gains to M²RNN’s non-linear state transition: in the homogeneous setting, M²RNN’s advantage is constrained by its smaller state size relative to Mamba-2 and Gated DeltaNet, however, in the hybrid setting, attention is responsible for in-context retrieval, allowing M²RNN’s non-linear recurrence to contribute expressivity that linear RNNs such as Mamba-2 and Gated DeltaNet cannot provide.

5.3.3 3-way Hybrid Models

We next explore 3-way hybrids that mix attention, Gated DeltaNet (or Mamba-2), and M²RNN layers. We find that replacing even a single linear RNN layer with M²RNN (denoted Hybrid Gated DeltaNet (or Mamba-2) + M²RNN-1) suffices to match the accuracy of the full Hybrid M²RNN model while preserving comparable training throughput (Section 5.7). This result indicates that M²RNN layers carry information that is substantially different from what Gated DeltaNet layers capture.

Hybrid Gated DeltaNet + M²RNN-1 improves upon Hybrid Gated DeltaNet, reducing Wikitext perplexity by 0.5 and 0.44 points at the 410M and 7B (1B active) scales, respectively. We also observe improvements on Hybrid Mamba-2 + M²RNN-1 over Hybrid Mamba-2 of 0.1 perplexity points on both model scales. Increasing the number of M²RNN layers to 3 (5 for 7B MoE) yields additional gains of 0.13 and 0.22 perplexity points. Together, these results solidify the importance of non-linear recurrences in sequence mixing blocks.

5.4 In-Context Retrieval

5.4.1 In-Context Retrieval on RULER

We evaluate the in-context retrieval ability of M²RNN relative to other linear RNNs on the RULER benchmark (Hsieh et al., 2024), focusing on the Single Needle In A Haystack (S-NIAH-1, 2, 3) (Nelson et al., 2024), Multi-Query (MQ), Multi-Key (MK), and Multi-Value (MV) variants:

1. **S-NIAH:** A key-value pair is embedded in context and the model is tasked to retrieve the value given the key. S-NIAH-1 uses a synthetic passage with word keys and numeric values, probing long-term retention. S-NIAH-2 and S-NIAH-3 use real-world essays with numeric and UUID values, respectively, testing efficient long-context memory management (Yang et al., 2024a).
2. **MQ-NIAH:** In the MQ-NIAH benchmark, multiple key-value pairs are embedded within the passage, and the task requires retrieving all needles associated with distinct keys.
3. **MK-NIAH:** The MK-NIAH benchmark inserts multiple key-value pairs in the passage. The task is to retrieve a single specified key while the other keys serve as distractors.
4. **MV-NIAH:** Multiple values share the same key and the model must retrieve all values associated with that key.

Figures 6 and 7 report accuracy at the 410M scale for Gated DeltaNet and Mamba-2-based models, respectively; Figures 8 and 9 report the same for the 7B (1B active) MoE model. All models are trained with a 4,096 context length and evaluated up to 16,384.

Hybrid Gated DeltaNet + M²RNN: Replacing a few Gated DeltaNet layers with M²RNN layers in the hybrid setting significantly improves retrieval at unseen context lengths on S-NIAH-2, and MQ/MK/MV-NIAH at the 410M parameter scale (Figure 6). At the 7B MoE scale, we observe that the 3-way consistently improves over the 2-way hybrid models except on S-NIAH-1 (Figure 8). Notably, augmenting with M²RNN layers also improves MQ/MK/MV-NIAH accuracy at context lengths seen during training ($\leq 4,096$) at both model scales.

On S-NIAH-1, we find that both Hybrid M²RNN and Hybrid Gated DeltaNet achieve 100% accuracy across all context lengths, however, adding M²RNN layers leads to accuracy degradation, likely due to the extremely synthetic passages used in the S-NIAH-1 task.

Hybrid Mamba-2 + M²RNN: We find that a single M²RNN layer with Hybrid Mamba-2 (Hybrid Mamba-2 + M²RNN-1) is insufficient to improve long-context retrieval at either model scale. However, replacing three Mamba-2 layers with M²RNN layers at 410M and 5 layers at 7B MoE yields consistent improvement (Figures 7, 9). We attribute this to the weaker state transition of Mamba-2 requiring more M²RNN layers to compensate.

Model	SQuAD	NQ	DROP	TriviaQA	FDA	SWDE	Avg
Mamba-2	31.2	15.0	19.5	50.5	15.6	32.4	27.4
Gated DeltaNet	34.8	15.4	24.9	51.7	16.3	41.8	<u>30.8</u>
RNN	9.6	5.9	14.6	29.7	0.0	5.0	<u>10.8</u>
GRU	15.8	8.8	17.2	41.5	0.7	7.7	15.3
M ² RNN	34.0	13.0	22.9	52.3	10.6	28.5	26.9
Transformer++	14.0	15.5	28.2	52.4	46.0	51.7	34.6
Hybrid Mamba-2	37.6	21.4	26.4	51.7	65.3	61.7	44.0
Hybrid Gated DeltaNet	37.6	22.2	26.0	53.4	61.5	58.0	43.1
Hybrid M ² RNN	41.3	22.7	26.8	55.5	74.5	60.7	46.9
Hybrid Mamba-2	37.6	21.4	26.4	51.7	65.3	61.7	44.0
Hybrid Mamba-2 + M ² RNN-1	38.6	23.8	26.3	55.7	61.3	60.2	44.3
Hybrid Mamba-2 + M ² RNN-3	40.4	23.5	26.4	56.7	65.2	61.7	<u>45.6</u>
Hybrid Gated DeltaNet	37.6	22.2	26.0	53.4	61.5	58.0	43.1
Hybrid Gated DeltaNet + M ² RNN-1	39.8	23.5	25.6	54.6	67.2	62.5	<u>45.5</u>
Hybrid Gated DeltaNet + M ² RNN-3	39.3	21.4	27.2	54.9	65.1	56.5	44.1

Table 3 In-context retrieval performance on real-world data at the 410M parameter scale.

Model	SQuAD	NQ	DROP	TriviaQA	FDA	SWDE	Avg
Mamba-2	41.7	26.5	30.0	65.0	33.0	54.4	41.8
Gated DeltaNet	40.3	24.2	29.9	64.3	32.4	61.8	<u>42.2</u>
RNN	20.0	12.2	20.4	53.1	0.8	9.8	19.4
GRU	27.0	16.7	24.6	59.3	5.2	18.4	25.2
M ² RNN	37.9	21.1	28.2	62.5	27.6	49.9	37.9
Transformer++	22.1	24.0	27.6	62.2	67.0	70.1	45.5
Hybrid Mamba-2	48.2	31.4	32.7	67.9	73.1	77.1	55.1
Hybrid Gated DeltaNet	46.4	31.2	28.3	63.6	67.1	71.9	51.4
Hybrid M ² RNN	48.4	31.4	31.4	64.6	78.0	79.8	55.6
Hybrid Mamba-2	48.2	31.4	32.7	67.9	73.1	77.1	55.1
Hybrid Mamba-2 + M ² RNN-1	46.6	30.6	33.6	67.1	78.4	75.0	<u>55.2</u>
Hybrid Mamba-2 + M ² RNN-5	46.8	31.5	28.7	66.0	78.5	79.7	<u>55.2</u>
Hybrid Gated DeltaNet	46.4	31.2	28.3	63.6	67.1	71.9	51.4
Hybrid Gated DeltaNet + M ² RNN-1	46.4	29.6	32.1	66.4	73.1	77.4	54.2
Hybrid Gated DeltaNet + M ² RNN-5	47.1	32.0	31.2	65.5	77.2	77.9	<u>55.1</u>

Table 4 In-context retrieval performance on real-world data at the 7B (1B active) MoE scale.

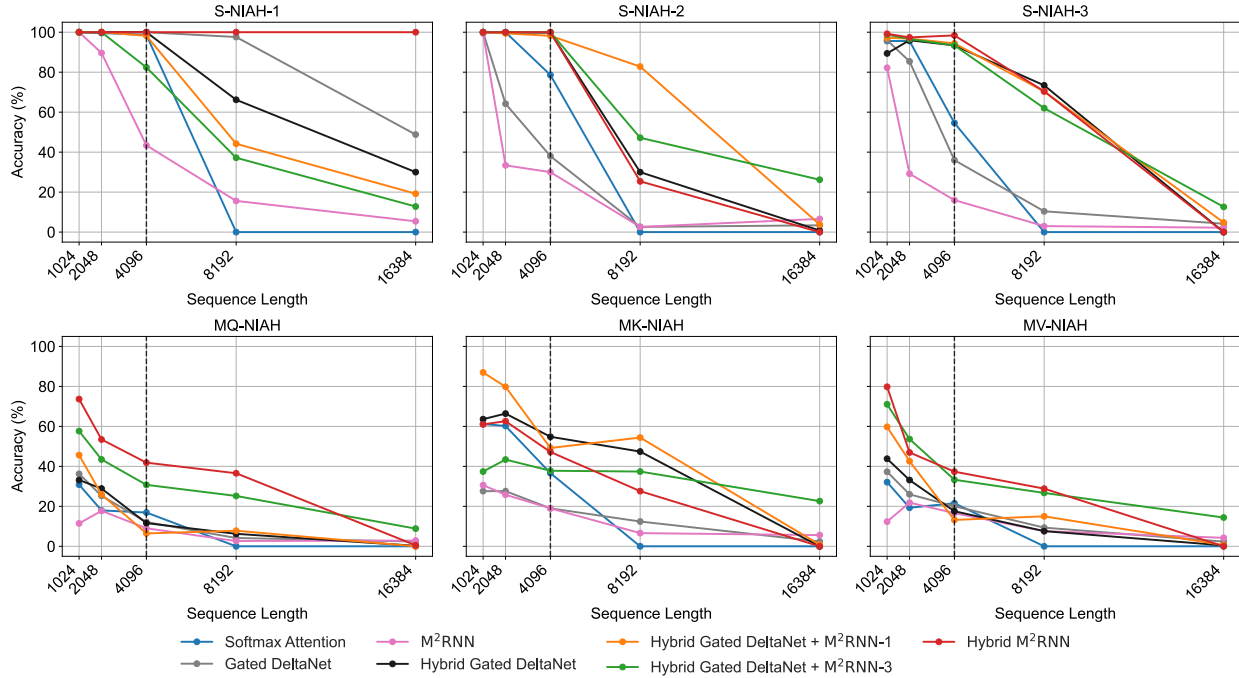


Figure 6 Zero-shot in-context retrieval performance on the RULER benchmark for M^2RNN layers and Gated DeltaNet models on 410M parameter scale. The vertical lines at 4096 indicate the training context length.

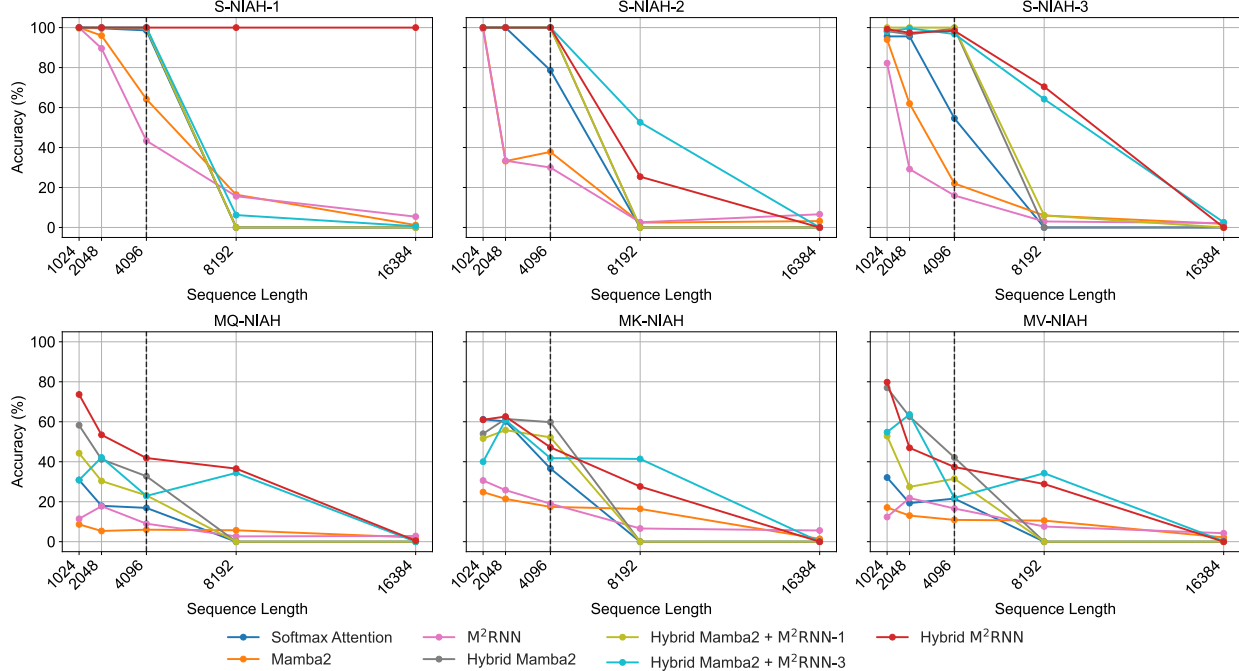


Figure 7 Zero-shot in-context retrieval performance on the RULER benchmark for M^2RNN layers and Mamba-2 models on 410M parameter scale. The vertical lines at 4096 indicate the training context length.

5.4.2 In-Context Retrieval on Real-World Data

Yang et al. (2024b) show that despite strong synthetic-task performance, DeltaNet still underperforms Mamba-2 (Dao and Gu, 2024) on real-world retrieval. To assess whether this limitation persists for M^2RNN ,

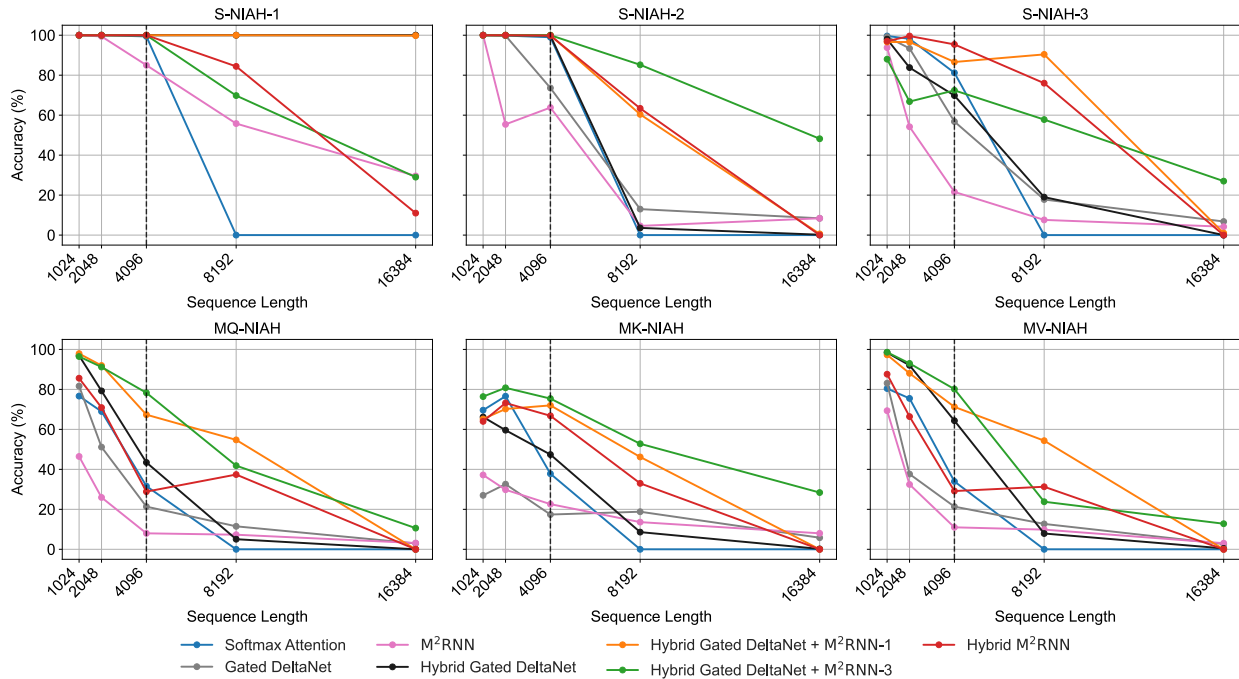


Figure 8 Zero-shot in-context retrieval performance on the RULER benchmark for M^2RNN layers and Gated DeltaNet models for the 7B MoE model. The vertical lines at 4096 indicate the training context length.

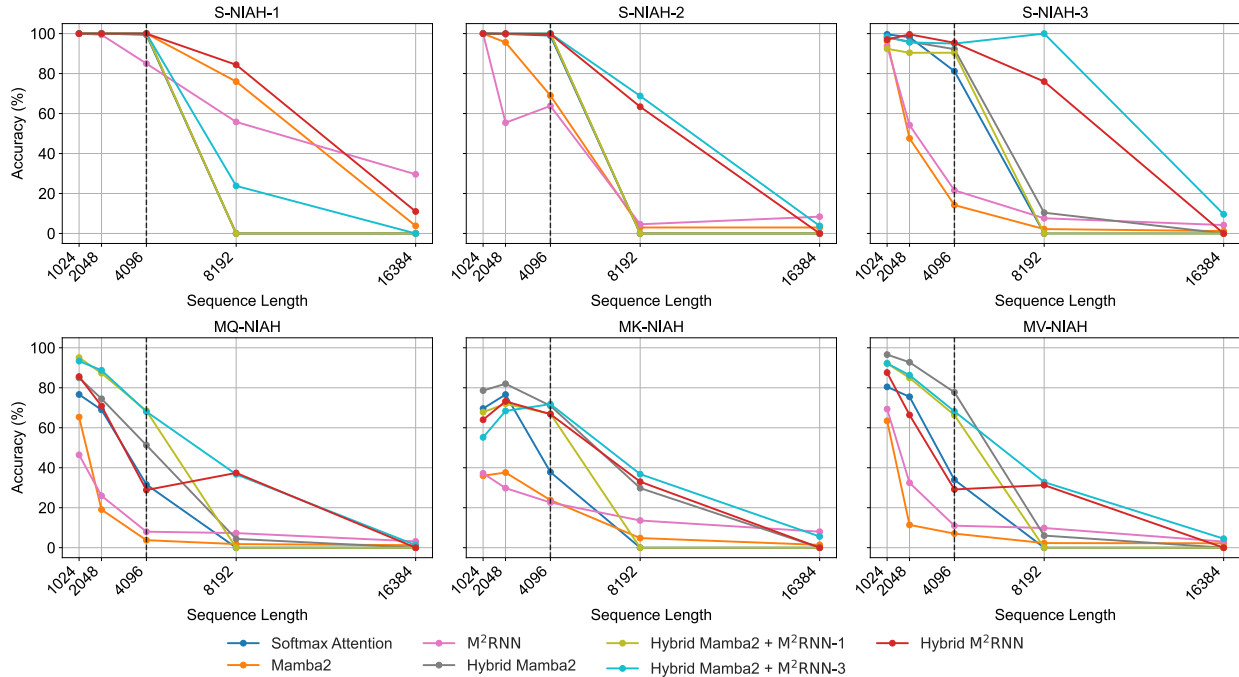


Figure 9 Zero-shot in-context retrieval performance on the RULER benchmark for M^2RNN layers and Mamba-2 models for the 7B MoE model. The vertical lines at 4096 indicate the training context length.

we evaluate in-context retrieval on real-world data for both model scales (Tables 3, 4).

As expected, Transformer++ (Vaswani et al., 2017) substantially outperforms all recurrent models due to its linearly growing key-value cache which helps with retrieval performance. Among purely recurrent architectures,

Gated DeltaNet (Yang et al., 2024a) outperforms Mamba-2 (Dao and Gu, 2024) and M²RNN which we attribute to the 3× larger state size of Gated DeltaNet. In the hybrid setting, all models significantly improve upon the Transformer++ baseline, with Hybrid M²RNN achieving the largest gains: 12.3 and 10.1 point gains across the 410M and 7B MoE model scales, outperforming both Hybrid Mamba-2 and Hybrid Gated DeltaNet. Further, we find that adding M²RNN layers to Hybrid Gated DeltaNet (Hybrid Gated DeltaNet + M²RNN) further improves upon Hybrid Gated DeltaNet. We observe similar improvements for Hybrid Mamba-2 when combined with M²RNN (Tables 3, 4).

5.5 Long-Context Performance

Model	GovReport	QMSum	MultiNews	TREC	TriviaQA	SAMSum	LCC	RepoBench-P	Avg
Mamba-2	6.6	14.3	9.9	26.5	23.2	11.5	13.7	8.9	14.3
Gated DeltaNet	7.6	18.2	12.0	19.0	34.1	21.3	14.9	11.8	<u>17.3</u>
RNN	9.3	15.2	9.2	0.5	12.2	5.0	17.9	14.9	10.5
GRU	7.0	16.5	10.8	1.0	21.4	8.5	12.5	9.0	10.8
M ² RNN	6.3	16.4	10.8	22.0	24.3	13.2	10.7	10.1	14.2
Transformer++	5.6	5.7	6.2	11.0	9.7	4.6	12.0	9.9	8.1
Hybrid Mamba-2	10.0	4.8	10.2	16.0	9.4	9.2	10.5	12.0	10.3
Hybrid Gated DeltaNet	8.2	16.8	16.1	19.5	28.7	15.9	8.7	9.2	<u>15.4</u>
Hybrid M ² RNN	10.0	14.0	7.2	17.5	35.5	14.9	13.4	10.3	<u>15.4</u>
Hybrid Mamba-2	10.0	4.8	10.2	16.0	9.4	9.2	10.5	12.0	10.3
Hybrid Mamba-2 + M ² RNN-1	9.8	9.0	7.5	22.5	13.3	12.6	13.2	9.8	12.2
Hybrid Mamba-2 + M ² RNN-3	10.5	15.8	13.2	29.0	31.7	12.1	10.7	13.3	<u>17.1</u>
Hybrid Gated DeltaNet	8.2	16.8	16.1	19.5	28.7	15.9	8.7	9.2	15.4
Hybrid Gated DeltaNet + M ² RNN-1	9.5	14.8	17.6	47.0	32.1	19.4	7.3	8.5	19.5
Hybrid Gated DeltaNet + M ² RNN-3	16.0	18.1	14.0	43.0	41.5	24.7	12.7	13.9	23.0

Table 5 Performance comparison on the 410M model across long-context summarization, coding and few-shot learning benchmarks.

Model	GovReport	QMSum	MultiNews	TREC	TriviaQA	SAMSum	LCC	RepoBench-P	Avg
Mamba-2	5.1	16.0	13.4	42.0	59.7	22.0	13.4	8.7	22.5
Gated DeltaNet	4.8	20.3	12.2	47.0	61.6	36.2	9.7	7.9	<u>25.0</u>
RNN	9.3	16.7	10.5	4.0	27.5	13.0	17.1	15.8	14.2
GRU	5.7	18.0	10.8	9.0	52.4	24.6	20.9	13.9	19.4
M ² RNN	8.1	19.1	11.8	26.5	51.3	30.7	20.4	19.3	23.4
Transformer++	6.1	6.1	17.0	16.0	11.4	10.0	13.1	10.2	11.2
Hybrid Mamba-2	9.1	7.7	20.3	62.5	23.3	12.1	5.6	9.8	18.8
Hybrid Gated DeltaNet	10.4	15.8	16.7	57.5	35.1	23.6	9.7	16.3	23.1
Hybrid M ² RNN	10.9	13.9	21.1	52.0	44.7	18.5	19.8	15.7	<u>24.6</u>
Hybrid Mamba-2	9.1	7.7	20.3	62.5	23.3	12.1	5.6	9.8	18.8
Hybrid Mamba-2 + M ² RNN-1	8.6	3.9	21.2	25.5	15.0	11.5	7.5	11.6	13.1
Hybrid Mamba-2 + M ² RNN-5	18.6	10.3	7.1	60.5	45.7	21.4	9.7	8.0	<u>22.7</u>
Hybrid Gated DeltaNet	10.4	15.8	16.7	57.5	35.1	23.6	9.7	16.3	23.1
Hybrid Gated DeltaNet + M ² RNN-1	17.2	16.5	6.0	69.5	64.9	34.1	20.1	15.1	30.4
Hybrid Gated DeltaNet + M ² RNN-5	12.2	16.0	16.1	59.0	73.5	36.0	18.0	18.9	31.2

Table 6 Performance comparison on the 7B (1B active) MoE model across long-context summarization, coding and few-shot learning benchmarks.

We evaluate long-context performance on LongBench (Bai et al., 2024) (Table 5, 6). In the 2-way hybrid setting, we find that Hybrid M²RNN matches Hybrid Gated DeltaNet at 410M parameter scale and outperforms Hybrid Gated DeltaNet by 1.5 points on the 7B MoE scale. We find that combining M²RNN layer with Hybrid Gated DeltaNet results in up to 8 points of average accuracy improvement across both model scales across long-context summarization, coding, and few-shot learning tasks. Similar improvements are observable with Hybrid Mamba-2 + M²RNN-3 (5 for 7B MoE) models on both model scales.

5.6 Ablations: Effect of State Size and Forget Gate

We ablate the contributions of state size and the forget gate on the recurrent model performance (Table 7). First, we compare a traditional vector-valued RNN (406M parameters) against M²RNN (410M parameters). The matrix-valued M²RNN model outperforms the vector-valued RNN by more than 10 perplexity points on WikiText (Merity et al., 2017) and 280 points on LAMBADA (Paperno et al., 2016), underscoring the critical role of state size.

Model	Wiki PPL	Lambada PPL	state size
RNN-406M	33.74	317.38	1,360
GRU-474M	25.80	63.83	1,360
M ² RNN-410M	22.92	33.63	86,016

Table 7 Perplexity comparison for RNN, GRU and M²RNN models with different state sizes.

To disentangle the effect of gating from that of state size, we additionally train GRU (Cho et al., 2014a) models with the same state dimensions as the vector-valued RNN. Despite having 16% more parameters (474M) due to the additional reset gate, GRUs still underperform M²RNN by 3 perplexity points on WikiText and 30 points on LAMBADA. These results confirm that expanding the state size is the primary driver of performance improvements in recurrent architectures, with gating mechanisms potentially providing further gains.

5.7 Training Throughput

We measure training throughput for M²RNN, Gated DeltaNet (Yang et al., 2024a), Mamba-2 (Dao and Gu, 2024), and Transformer++ on 8× NVIDIA HGX H100 GPUs connected via NVLink, using our 7B (1B active) MoE configuration. As shown in Figure 10, Mamba-2 consistently achieves the highest throughput across context lengths, while Transformer++ degrades significantly at longer contexts due to its quadratic complexity.

Although M²RNN has linear time complexity, its higher constant factors make it more expensive than the linear baselines in the homogeneous setting. However, replacing a single Gated DeltaNet layer with M²RNN layer to the Hybrid Gated DeltaNet model (Hybrid Gated DeltaNet + M²RNN-1) achieves throughput comparable to Hybrid Gated DeltaNet alone (within 6% at 16k context length) while consistently improving model quality across all benchmarks. We consider this a favorable tradeoff, making M²RNN layers practical when used sparingly. Our current implementation is based on the Triton DSL (Tillet et al., 2019) and is relatively unoptimized, leaving significant room for improvement that could further narrow the remaining throughput gap.

6 Conclusion

We introduce Matrix-to-Matrix RNN (M²RNN), a non-linear RNN architecture with matrix-valued hidden states that addresses key limitations of existing linear recurrent models. By combining expressive non-linear state transitions with a forget gate and an outer product state expansion, M²RNN achieves strong state-tracking capabilities.

Our experiments demonstrate that M²RNN consistently comes close to Mamba-2 (Dao and Gu, 2024) and Gated DeltaNet (Yang et al., 2024a) at both the 410M dense and 7B (1B active) MoE scales. More importantly, hybrid models combining M²RNN with attention layers significantly outperform equivalent Mamba-2 and Gated DeltaNet hybrids in language modeling, in-context retrieval, and long-context generalization. We further show that even a single M²RNN layer yields substantial accuracy gains with only 6% throughput degradation, making it a practical enhancement for existing architectures.

The matrix-valued recurrence in M²RNN eliminates the FLOPs wasted by padding in vector-valued recurrences when using the FlashRNN algorithm (Pöppel et al., 2025), enabling efficient tensor core utilization independent of batch size. Combined with our custom kernels, this makes M²RNN a viable component for training state-of-the-art production language models.

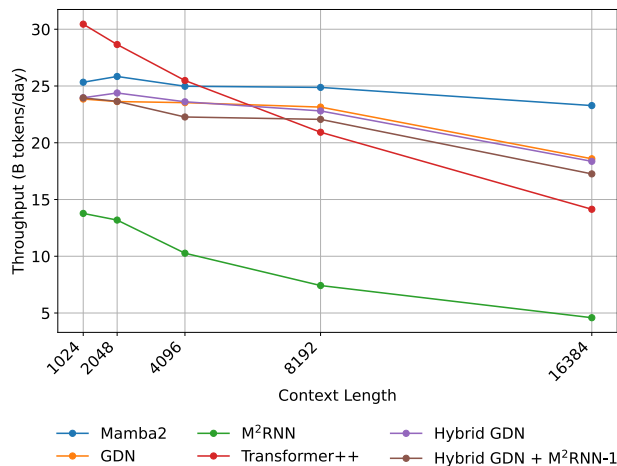


Figure 10 Training throughput measured in billion tokens per day on a machine with 8x NVIDIA HGX H100 GPUs for our 7B MoE configuration.

We also present two complementary tensor parallelism strategies for M²RNN. The topology-aware approach adopts a grouped-value formulation that requires no additional communication beyond standard TP, while the topology-independent approach preserves the parameter count regardless of TP world size at the cost of a small number of extra AllReduce operations. Together, these strategies make M²RNN readily deployable across diverse multi-GPU configurations.

Limitations and Future Work. The non-linear recurrence introduces additional computational overhead compared to linear alternatives. Future work could explore approximations or more efficient kernel implementations to reduce this cost while preserving expressivity. Additionally, evaluating M²RNN at larger scales and with longer training contexts would further validate its potential as a foundational building block for efficient language models.

Acknowledgement

We would like to thank Songlin Yang, Bharat Runwal and Kevin Li for providing valuable feedback and discussion throughout the duration of this project. We gratefully acknowledge the support of the Schmidt Sciences AI2050 fellowship, the Google ML and Systems Junior Faculty Awards, and the Google Research Scholar program.

References

Jason Ansel, Edward Yang, Horace He, Natalia Gimelshein, Animesh Jain, Michael Voznesensky, Bin Bao, Peter Bell, David Berard, Evgeni Burovski, Geeta Chauhan, Anjali Chourdia, Will Constable, Alban Desmaison, Zachary DeVito, Elias Ellison, Will Feng, Jiong Gong, Michael Gschwind, Brian Hirsh, Sherlock Huang, Kshiteej Kalambarakar, Laurent Kirsch, Michael Lazos, Mario Lezcano, Yanbo Liang, Jason Liang, Yinghai Lu, C. K. Luk, Bert Maher, Yunjie Pan, Christian Puhersch, Matthias Reso, Mark Saroufim, Marcos Yukio Siraichi, Helen Suk, Shunting Zhang, Michael Suo, Phil Tillet, Xu Zhao, Eikan Wang, Keren Zhou, Richard Zou, Xiaodong Wang, Ajit Mathews, William Wen, Gregory Chanan, Peng Wu, and Soumith Chintala. Pytorch 2: Faster machine learning through dynamic python bytecode transformation and graph compilation. In *Proceedings of the 29th ACM International Conference on Architectural Support for Programming Languages and Operating Systems, Volume 2, ASPLOS '24*, page 929–947, New York, NY, USA, 2024. Association for Computing Machinery. ISBN 9798400703850. doi: 10.1145/3620665.3640366. <https://doi.org/10.1145/3620665.3640366>.

Yushi Bai, Xin Lv, Jiajie Zhang, Hongchang Lyu, Jiankai Tang, Zhidian Huang, Zhengxiao Du, Xiao Liu, Aohan Zeng, Lei Hou, et al. Longbench: A bilingual, multitask benchmark for long context understanding. In *Proceedings of the*

- 62nd annual meeting of the association for computational linguistics (volume 1: Long papers), pages 3119–3137, 2024.
- Maximilian Beck, Korbinian Pöppel, Markus Spanring, Andreas Auer, Oleksandra Prudnikova, Michael Kopp, Günter Klambauer, Johannes Brandstetter, and Sepp Hochreiter. xlstm: Extended long short-term memory. *Advances in Neural Information Processing Systems*, 37:107547–107603, 2024.
- Y. Bengio, P. Simard, and P. Frasconi. Learning long-term dependencies with gradient descent is difficult. *IEEE Transactions on Neural Networks*, 5(2):157–166, 1994. doi: 10.1109/72.279181.
- Yonatan Bisk, Rowan Zellers, Ronan Le Bras, Jianfeng Gao, and Yejin Choi. Piqa: Reasoning about physical commonsense in natural language, 2019. <https://arxiv.org/abs/1911.11641>.
- Aaron Blakeman, Aaron Grattafiori, Aarti Basant, Abhibha Gupta, Abhinav Khattar, Adi Renduchintala, Aditya Vavre, Akanksha Shukla, Akhiad Bercovich, Aleksander Ficek, et al. Nvidia nemotron 3: Efficient and open intelligence. *arXiv preprint arXiv:2512.20856*, 2025.
- Guy E. Blelloch. Prefix sums and their applications. Technical Report CMU-CS-90-190, School of Computer Science, Carnegie Mellon University, November 1990.
- Tom Brown, Benjamin Mann, Nick Ryder, Melanie Subbiah, Jared D Kaplan, Prafulla Dhariwal, Arvind Neelakantan, Pranav Shyam, Girish Sastry, Amanda Askell, et al. Language models are few-shot learners. *Advances in neural information processing systems*, 33:1877–1901, 2020.
- Kyunghyun Cho, Bart Van Merriënboer, Dzmitry Bahdanau, and Yoshua Bengio. On the properties of neural machine translation: Encoder-decoder approaches. *arXiv preprint arXiv:1409.1259*, 2014a.
- Kyunghyun Cho, Bart Van Merriënboer, Caglar Gulcehre, Dzmitry Bahdanau, Fethi Bougares, Holger Schwenk, and Yoshua Bengio. Learning phrase representations using rnn encoder-decoder for statistical machine translation. *arXiv preprint arXiv:1406.1078*, 2014b.
- Aakanksha Chowdhery, Sharan Narang, Jacob Devlin, Maarten Bosma, Gaurav Mishra, Adam Roberts, Paul Barham, Hyung Won Chung, Charles Sutton, Sebastian Gehrmann, et al. Palm: Scaling language modeling with pathways. *Journal of Machine Learning Research*, 24(240):1–113, 2023.
- Junyoung Chung, Caglar Gulcehre, KyungHyun Cho, and Yoshua Bengio. Empirical evaluation of gated recurrent neural networks on sequence modeling. *arXiv preprint arXiv:1412.3555*, 2014.
- Christopher Clark, Kenton Lee, Ming-Wei Chang, Tom Kwiatkowski, Michael Collins, and Kristina Toutanova. Boolq: Exploring the surprising difficulty of natural yes/no questions, 2019. <https://arxiv.org/abs/1905.10044>.
- Peter Clark, Isaac Cowhey, Oren Etzioni, Tushar Khot, Ashish Sabharwal, Carissa Schoenick, and Oyvind Tafjord. Think you have solved question answering? try arc, the ai2 reasoning challenge, 2018. <https://arxiv.org/abs/1803.05457>.
- Federico Danieli, Pau Rodriguez, Miguel Sarabia, Xavier Suau, and Luca Zappella. Pararnn: Unlocking parallel training of nonlinear rnns for large language models. *arXiv preprint arXiv:2510.21450*, 2025.
- Tri Dao. Flashattention-2: Faster attention with better parallelism and work partitioning. *arXiv preprint arXiv:2307.08691*, 2023.
- Tri Dao and Albert Gu. Transformers are ssms: Generalized models and efficient algorithms through structured state space duality. *arXiv preprint arXiv:2405.21060*, 2024.
- Tri Dao, Dan Fu, Stefano Ermon, Atri Rudra, and Christopher Ré. Flashattention: Fast and memory-efficient exact attention with io-awareness. *Advances in neural information processing systems*, 35:16344–16359, 2022.
- Alexey Dosovitskiy. An image is worth 16x16 words: Transformers for image recognition at scale. *arXiv preprint arXiv:2010.11929*, 2020.
- Stefan Elfving, Eiji Uchibe, and Kenji Doya. Sigmoid-weighted linear units for neural network function approximation in reinforcement learning. *Neural networks*, 107:3–11, 2018.
- Jeffrey L Elman. Finding structure in time. *Cognitive science*, 14(2):179–211, 1990.
- Daniel Y Fu, Tri Dao, Khaled K Saab, Armin W Thomas, Atri Rudra, and Christopher Ré. Hungry hungry hippos: Towards language modeling with state space models. *arXiv preprint arXiv:2212.14052*, 2022.
- Leo Gao, Jonathan Tow, Baber Abbasi, Stella Biderman, Sid Black, Anthony DiPofi, Charles Foster, Laurence Golding, Jeffrey Hsu, Alain Le Noac’h, Haonan Li, Kyle McDonell, Niklas Muennighoff, Chris Ociepa, Jason Phang, Laria

Reynolds, Hailey Schoelkopf, Aviya Skowron, Lintang Sutawika, Eric Tang, Anish Thite, Ben Wang, Kevin Wang, and Andy Zou. The language model evaluation harness, 07 2024. <https://zenodo.org/records/12608602>.

Aaron Grattafiori, Abhimanyu Dubey, Abhinav Jauhri, Abhinav Pandey, Abhishek Kadian, Ahmad Al-Dahle, Aiesha Letman, Akhil Mathur, Alan Schelten, Alex Vaughan, Amy Yang, Angela Fan, Anirudh Goyal, Anthony Hartshorn, Aobo Yang, Archi Mitra, Archie Sravankumar, Artem Korenev, Arthur Hinsvark, Arun Rao, Aston Zhang, Aurelien Rodriguez, Austen Gregerson, Ava Spataru, Baptiste Roziere, Bethany Biron, Binh Tang, Bobbie Chern, Charlotte Caucheteux, Chaya Nayak, Chloe Bi, Chris Marra, Chris McConnell, Christian Keller, Christophe Touret, Chunyang Wu, Corinne Wong, Cristian Canton Ferrer, Cyrus Nikolaidis, Damien Allonsius, Daniel Song, Danielle Pintz, Danny Livshits, Danny Wyatt, David Esiobu, Dhruv Choudhary, Dhruv Mahajan, Diego Garcia-Olano, Diego Perino, Dieuwke Hupkes, Egor Lakomkin, Ehab AlBadawy, Elina Lobanova, Emily Dinan, Eric Michael Smith, Filip Radenovic, Francisco Guzmán, Frank Zhang, Gabriel Synnaeve, Gabrielle Lee, Georgia Lewis Anderson, Govind Thattai, Graeme Nail, Gregoire Mialon, Guan Pang, Guillem Cucurell, Hailey Nguyen, Hannah Korevaar, Hu Xu, Hugo Touvron, Iliyan Zarov, Imanol Arrieta Ibarra, Isabel Kloumann, Ishan Misra, Ivan Evtimov, Jack Zhang, Jade Copet, Jaewon Lee, Jan Geffert, Jana Vranes, Jason Park, Jay Mahadeokar, Jeet Shah, Jelmer van der Linde, Jennifer Billock, Jenny Hong, Jenya Lee, Jeremy Fu, Jianfeng Chi, Jianyu Huang, Jiawen Liu, Jie Wang, Jiecao Yu, Joanna Bitton, Joe Spisak, Jongsoo Park, Joseph Rocca, Joshua Johnstun, Joshua Saxe, Junteng Jia, Kalyan Vasuden Alwala, Karthik Prasad, Kartikeya Upasani, Kate Plawiak, Ke Li, Kenneth Heafield, Kevin Stone, Khalid El-Arini, Krithika Iyer, Kshitiz Malik, Kuenley Chiu, Kunal Balla, Kushal Lakhotia, Lauren Rantala-Yeara, Laurens van der Maaten, Lawrence Chen, Liang Tan, Liz Jenkins, Louis Martin, Lovish Madaan, Lubo Malo, Lukas Blecher, Lukas Landzaat, Luke de Oliveira, Madeline Muzzi, Mahesh Pasupuleti, Mannat Singh, Manohar Paluri, Marcin Kardas, Maria Tsimpoukelli, Mathew Oldham, Mathieu Rita, Maya Pavlova, Melanie Kambadur, Mike Lewis, Min Si, Mitesh Kumar Singh, Mona Hassan, Naman Goyal, Narjes Torabi, Nikolay Bashlykov, Nikolay Bogoychev, Niladri Chatterji, Ning Zhang, Olivier Duchenne, Onur Çelebi, Patrick Alrassy, Pengchuan Zhang, Pengwei Li, Petar Vasic, Peter Weng, Prajjwal Bhargava, Pratik Dubal, Praveen Krishnan, Punit Singh Koura, Puxin Xu, Qing He, Qingxiao Dong, Ragavan Srinivasan, Raj Ganapathy, Ramon Calderer, Ricardo Silveira Cabral, Robert Stojnic, Roberta Raileanu, Rohan Maheswari, Rohit Girdhar, Rohit Patel, Romain Sauvestre, Ronnie Polidoro, Roshan Sumbaly, Ross Taylor, Ruan Silva, Rui Hou, Rui Wang, Saghar Hosseini, Sahana Chennabasappa, Sanjay Singh, Sean Bell, Seohyun Sonia Kim, Sergey Edunov, Shaoliang Nie, Sharan Narang, Sharath Rparathy, Sheng Shen, Shengye Wan, Shruti Bhosale, Shun Zhang, Simon Vandenhende, Soumya Batra, Spencer Whitman, Sten Sootla, Stephane Collet, Suchin Gururangan, Sydney Borodinsky, Tamar Herman, Tara Fowler, Tarek Sheasha, Thomas Georgiou, Thomas Scialom, Tobias Speckbacher, Todor Mihaylov, Tong Xiao, Ujjwal Karn, Vedanuj Goswami, Vibhor Gupta, Vignesh Ramanathan, Viktor Kerkez, Vincent Gonguet, Virginie Do, Vish Vogeti, Vitor Albiero, Vladan Petrovic, Weiwei Chu, Wenhan Xiong, Wenyin Fu, Whitney Meers, Xavier Martinet, Xiaodong Wang, Xiaofang Wang, Xiaoqing Ellen Tan, Xide Xia, Xinfeng Xie, Xuchao Jia, Xuwei Wang, Yaelle Goldschlag, Yashesh Gaur, Yasmine Babaei, Yi Wen, Yiwen Song, Yuchen Zhang, Yue Li, Yuning Mao, Zacharie Delpierre Coudert, Zheng Yan, Zhengxing Chen, Zoe Papanikos, Aaditya Singh, Aayushi Srivastava, Abha Jain, Adam Kelsey, Adam Shajnfeld, Adithya Gangidi, Adolfo Victoria, Ahuva Goldstand, Ajay Menon, Ajay Sharma, Alex Boesenberg, Alexei Baevski, Allie Feinstein, Amanda Kallet, Amit Sangani, Amos Teo, Anam Yunus, Andrei Lupu, Andres Alvarado, Andrew Caples, Andrew Gu, Andrew Ho, Andrew Poulton, Andrew Ryan, Ankit Ramchandani, Annie Dong, Annie Franco, Anuj Goyal, Aparajita Saraf, Arkabandhu Chowdhury, Ashley Gabriel, Ashwin Barambe, Assaf Eisenman, Azadeh Yazdan, Beau James, Ben Maurer, Benjamin Leonhardi, Bernie Huang, Beth Loyd, Beto De Paola, Bhargavi Paranjape, Bing Liu, Bo Wu, Boyu Ni, Braden Hancock, Bram Wasti, Brandon Spence, Brani Stojkovic, Brian Gamido, Britt Montalvo, Carl Parker, Carly Burton, Catalina Mejia, Ce Liu, Changhan Wang, Changkyu Kim, Chao Zhou, Chester Hu, Ching-Hsiang Chu, Chris Cai, Chris Tindal, Christoph Feichtenhofer, Cynthia Gao, Damon Civin, Dana Beaty, Daniel Kreymer, Daniel Li, David Adkins, David Xu, Davide Testuggine, Delia David, Devi Parikh, Diana Liskovich, Didem Foss, Ding Kang Wang, Duc Le, Dustin Holland, Edward Dowling, Eissa Jamil, Elaine Montgomery, Eleonora Presani, Emily Hahn, Emily Wood, Eric-Tuan Le, Erik Brinkman, Esteban Arcaute, Evan Dunbar, Evan Smothers, Fei Sun, Felix Kreuk, Feng Tian, Filippos Kokkinos, Firat Ozgenel, Francesco Caggioni, Frank Kanayet, Frank Seide, Gabriela Medina Florez, Gabriella Schwarz, Gada Badeer, Georgia Swee, Gil Halpern, Grant Herman, Grigory Sizov, Guangyi, Zhang, Guna Lakshminarayanan, Hakan Inan, Hamid Shojanazeri, Han Zou, Hannah Wang, Hanwen Zha, Haroun Habeeb, Harrison Rudolph, Helen Suk, Henry Aspegren, Hunter Goldman, Hongyuan Zhan, Ibrahim Damla, Igor Molybog, Igor Tufanov, Ilias Leontiadis, Irina-Elena Veliche, Itai Gat, Jake Weissman, James Geboski, James Kohli, Janice Lam, Japhet Asher, Jean-Baptiste Gaya, Jeff Marcus, Jeff Tang, Jennifer Chan, Jenny Zhen, Jeremy Reizenstein, Jeremy Teboul, Jessica Zhong, Jian Jin, Jingyi Yang, Joe Cummings, Jon Carvill, Jon Shepard, Jonathan McPhie, Jonathan Torres, Josh Ginsburg, Junjie Wang, Kai Wu, Kam Hou U, Karan Saxena, Kartikay Khandelwal, Katayoun Zand, Kathy Matosich, Kaushik Veeraraghavan, Kelly Michelena, Keqian Li, Kiran Jagadeesh, Kun Huang, Kunal Chawla, Kyle Huang, Lailin Chen, Lakshya Garg, Lavender A, Leandro Silva, Lee Bell, Lei Zhang, Liangpeng Guo, Licheng Yu, Liron Moshkovich, Luca Wehrstedt, Madian Khabsa, Manav Avalani, Manish Bhatt, Martynas Mankus, Matan Hasson, Matthew Lennie, Matthias

- Reso, Maxim Groshev, Maxim Naumov, Maya Lathi, Meghan Keneally, Miao Liu, Michael L. Seltzer, Michal Valko, Michelle Restrepo, Mihir Patel, Mik Vyatskov, Mikayel Samvelyan, Mike Clark, Mike Macey, Mike Wang, Miquel Jubert Hermoso, Mo Metanat, Mohammad Rastegari, Munish Bansal, Nandhini Santhanam, Natascha Parks, Natasha White, Navyata Bawa, Nayan Singhal, Nick Egebo, Nicolas Usunier, Nikhil Mehta, Nikolay Pavlovich Laptev, Ning Dong, Norman Cheng, Oleg Chernoguz, Olivia Hart, Omkar Salpekar, Ozlem Kalinli, Parkin Kent, Parth Parekh, Paul Saab, Pavan Balaji, Pedro Rittner, Philip Bontrager, Pierre Roux, Piotr Dollar, Polina Zvyagina, Prashant Ratanandani, Pritish Yuvraj, Qian Liang, Rachad Alao, Rachel Rodriguez, Rafi Ayub, Raghotham Murthy, Raghu Nayani, Rahul Mitra, Rangaprabhu Parthasarathy, Raymond Li, Rebekkah Hogan, Robin Battey, Rocky Wang, Russ Howes, Ruty Rinott, Sachin Mehta, Sachin Siby, Sai Jayesh Bondu, Samyak Datta, Sara Chugh, Sara Hunt, Sargun Dhillon, Sasha Sidorov, Satadru Pan, Saurabh Mahajan, Saurabh Verma, Seiji Yamamoto, Sharadh Ramaswamy, Shaun Lindsay, Sheng Feng, Shenghao Lin, Shengxin Cindy Zha, Shishir Patil, Shiva Shankar, Shuqiang Zhang, Sinong Wang, Sneha Agarwal, Soji Sajuyigbe, Soumith Chintala, Stephanie Max, Stephen Chen, Steve Kehoe, Steve Satterfield, Sudarshan Govindaprasad, Sumit Gupta, Summer Deng, Sungmin Cho, Sunny Virk, Suraj Subramanian, Sy Choudhury, Sydney Goldman, Tal Remez, Tamar Glaser, Tamara Best, Thilo Koehler, Thomas Robinson, Tianhe Li, Tianjun Zhang, Tim Matthews, Timothy Chou, Tzook Shaked, Varun Vontimitta, Victoria Ajayi, Victoria Montanez, Vijai Mohan, Vinay Satish Kumar, Vishal Mangla, Vlad Ionescu, Vlad Poenaru, Vlad Tiberiu Mihailescu, Vladimir Ivanov, Wei Li, Wenchen Wang, Wenwen Jiang, Wes Bouaziz, Will Constable, Xiaocheng Tang, Xiaoqian Wu, Xiaolan Wang, Xilun Wu, Xinbo Gao, Yaniv Kleinman, Yanjun Chen, Ye Hu, Ye Jia, Ye Qi, Yenda Li, Yilin Zhang, Ying Zhang, Yossi Adi, Youngjin Nam, Yu, Wang, Yu Zhao, Yuchen Hao, Yundi Qian, Yunlu Li, Yuzi He, Zach Rait, Zachary DeVito, Zef Rosnbrick, Zhaoduo Wen, Zhenyu Yang, Zhiwei Zhao, and Zhiyu Ma. The llama 3 herd of models, 2024. <https://arxiv.org/abs/2407.21783>.
- Riccardo Grazi, Julien Siems, Arber Zela, Jörg KH Franke, Frank Hutter, and Massimiliano Pontil. Unlocking state-tracking in linear rnns through negative eigenvalues. *arXiv preprint arXiv:2411.12537*, 2024.
- Albert Gu and Tri Dao. Mamba: Linear-time sequence modeling with selective state spaces. In *First conference on language modeling*, 2024.
- Albert Gu, Karan Goel, and Christopher Ré. Efficiently modeling long sequences with structured state spaces. *arXiv preprint arXiv:2111.00396*, 2021a.
- Albert Gu, Isys Johnson, Karan Goel, Khaled Saab, Tri Dao, Atri Rudra, and Christopher Ré. Combining recurrent, convolutional, and continuous-time models with linear state space layers. *Advances in neural information processing systems*, 34:572–585, 2021b.
- Wentao Guo, Mayank Mishra, Xinle Cheng, Ion Stoica, and Tri Dao. Sonicmoe: Accelerating moe with io and tile-aware optimizations. *arXiv preprint arXiv:2512.14080*, 2025.
- D Hendrycks. Gaussian error linear units (gelus). *arXiv preprint arXiv:1606.08415*, 2016.
- W. Daniel Hillis and Guy L. Steele. Data parallel algorithms. *Commun. ACM*, 29(12):1170–1183, December 1986. ISSN 0001-0782. doi: 10.1145/7902.7903. <https://doi.org/10.1145/7902.7903>.
- Sepp Hochreiter and Jürgen Schmidhuber. Long short-term memory. *Neural Computation*, 9(8):1735–1780, 1997. doi: 10.1162/neco.1997.9.8.1735.
- Cheng-Ping Hsieh, Simeng Sun, Samuel Kriman, Shantanu Acharya, Dima Rekeshe, Fei Jia, Yang Zhang, and Boris Ginsburg. Ruler: What’s the real context size of your long-context language models? *arXiv preprint arXiv:2404.06654*, 2024.
- Weizhe Hua, Zihang Dai, Hanxiao Liu, and Quoc Le. Transformer quality in linear time. In *International conference on machine learning*, pages 9099–9117. PMLR, 2022.
- IBM Granite Team. Granite 4.0 language models. <https://huggingface.co/collections/ibm-granite/granite-40-language-models>, 2025. Hugging Face collection, accessed January 28, 2026.
- Dhiraj Kalamkar, Dheevatsa Mudigere, Naveen Mellempudi, Dipankar Das, Kunal Banerjee, Sasikanth Avancha, Dharma Teja Vooturi, Nataraj Jammalamadaka, Jianyu Huang, Hector Yuen, et al. A study of bfloat16 for deep learning training. *arXiv preprint arXiv:1905.12322*, 2019.
- Angelos Katharopoulos, Apoorv Vyas, Nikolaos Pappas, and François Fleuret. Transformers are rnns: Fast autoregressive transformers with linear attention. In *International conference on machine learning*, pages 5156–5165. PMLR, 2020.
- Amirhossein Kazemnejad, Inkit Padhi, Karthikeyan Natesan Ramamurthy, Payel Das, and Siva Reddy. The impact of positional encoding on length generalization in transformers. *Advances in Neural Information Processing Systems*, 36:24892–24928, 2023.

- Quoc V. Le, Navdeep Jaitly, and Geoffrey E. Hinton. A simple way to initialize recurrent networks of rectified linear units, 2015. <https://arxiv.org/abs/1504.00941>.
- Opher Lieber, Barak Lenz, Hofit Bata, Gal Cohen, Jhonathan Osin, Itay Dalmedigos, Erez Safahi, Shaked Meirum, Yonatan Belinkov, Shai Shalev-Shwartz, et al. Jamba: A hybrid transformer-mamba language model. *arXiv preprint arXiv:2403.19887*, 2024.
- Aixin Liu, Bei Feng, Bing Xue, Bingxuan Wang, Bochao Wu, Chengda Lu, Chenggang Zhao, Chengqi Deng, Chenyu Zhang, Chong Ruan, et al. Deepseek-v3 technical report. *arXiv preprint arXiv:2412.19437*, 2024.
- Ilya Loshchilov and Frank Hutter. Decoupled weight decay regularization, 2019. <https://arxiv.org/abs/1711.05101>.
- Loren Lugosch, Mirco Ravanelli, Patrick Ignoto, Vikrant Singh Tomar, and Yoshua Bengio. Speech model pre-training for end-to-end spoken language understanding. *arXiv preprint arXiv:1904.03670*, 2019.
- Stephen Merity, Caiming Xiong, James Bradbury, and Richard Socher. Pointer sentinel mixture models. In *International Conference on Learning Representations*, 2017. <https://openreview.net/forum?id=Byj72udxe>.
- William Merrill. Sequential neural networks as automata. *arXiv preprint arXiv:1906.01615*, 2019.
- William Merrill, Ashish Sabharwal, and Noah A. Smith. Saturated transformers are constant-depth threshold circuits. *Transactions of the Association for Computational Linguistics*, 10:843–856, 2022. doi: 10.1162/tacl_a_00493. <https://aclanthology.org/2022.tacl-1.49/>.
- William Merrill, Jackson Petty, and Ashish Sabharwal. The illusion of state in state-space models. *arXiv preprint arXiv:2404.08819*, 2024.
- Meta AI. The llama 4 herd: The beginning of a new era of natively multimodal ai innovation, 2025. <https://ai.meta.com/blog/llama-4-multimodal-intelligence/>.
- Paulius Micikevicius, Sharan Narang, Jonah Alben, Gregory Diamos, Erich Elsen, David Garcia, Boris Ginsburg, Michael Houston, Oleksii Kuchaiev, Ganesh Venkatesh, et al. Mixed precision training. *arXiv preprint arXiv:1710.03740*, 2017.
- Todor Mihaylov, Peter Clark, Tushar Khot, and Ashish Sabharwal. Can a suit of armor conduct electricity? a new dataset for open book question answering, 2018. <https://arxiv.org/abs/1809.02789>.
- Mayank Mishra. Lm engine: A hyper-optimized library for pretraining and finetuning, 2024. <https://github.com/open-lm-engine/lm-engine>.
- Mayank Mishra, Matt Stallone, Gaoyuan Zhang, Yikang Shen, Aditya Prasad, Adriana Meza Soria, Michele Merler, Parameswaran Selvam, Saptha Surendran, Shivdeep Singh, et al. Granite code models: A family of open foundation models for code intelligence. *arXiv preprint arXiv:2405.04324*, 2024.
- Elliot Nelson, Georgios Kollias, Payel Das, Subhajit Chaudhury, and Soham Dan. Needle in the haystack for memory based large language models. *arXiv preprint arXiv:2407.01437*, 2024.
- NVIDIA, :, Aarti Basant, Abhijit Khairnar, Abhijit Paithankar, Abhinav Khattar, Adithya Renduchintala, Aditya Malte, Akhiad Bercovich, Akshay Hazare, Alejandra Rico, Aleksander Ficek, Alex Kondratenko, Alex Shaposhnikov, Alexander Bukharin, Ali Taghibakhshi, Amelia Barton, Ameya Sunil Mahabaleshwarkar, Amy Shen, Andrew Tao, Ann Guan, Anna Shors, Anubhav Mandarwal, Arham Mehta, Arun Venkatesan, Ashton Sharabiani, Ashwath Aithal, Ashwin Poojary, Ayush Dattagupta, Balaram Buddharaju, Banghua Zhu, Barnaby Simkin, Bilal Kartal, Bitu Darvish Rouhani, Bobby Chen, Boris Ginsburg, Brandon Norick, Brian Yu, Bryan Catanzaro, Charles Wang, Charlie Truong, Chetan Mungekar, Chintan Patel, Chris Alexiuk, Christian Munley, Christopher Parisien, Dan Su, Daniel Afrimi, Daniel Korzekwa, Daniel Rohrer, Daria Gitman, David Mosallanezhad, Deepak Narayanan, Dima Relesh, Dina Yared, Dmytro Pykhtar, Dong Ahn, Duncan Riach, Eileen Long, Elliott Ning, Eric Chung, Erick Galinkin, Evelina Bakhturina, Gargi Prasad, Gerald Shen, Haifeng Qian, Haim Elisha, Harsh Sharma, Hayley Ross, Helen Ngo, Herman Sahota, Hexin Wang, Hoo Chang Shin, Hua Huang, Iain Cunningham, Igor Gitman, Ivan Moshkov, Jaehun Jung, Jan Kautz, Jane Polak Scowcroft, Jared Casper, Jian Zhang, Jiaqi Zeng, Jimmy Zhang, Jinze Xue, Jocelyn Huang, Joey Conway, John Kamalu, Jonathan Cohen, Joseph Jennings, Julien Veron Vialard, Junkeun Yi, Jupinder Parmar, Kari Briski, Katherine Cheung, Katherine Luna, Keith Wyss, Keshav Santhanam, Kezhi Kong, Krzysztof Pawelec, Kumar Anik, Kunlun Li, Kushan Ahmadian, Lawrence McAfee, Laya Sleiman, Leon Derczynski, Luis Vega, Maer Rodrigues de Melo, Makesh Narsimhan Sreedhar, Marcin Chochowski, Mark Cai, Markus Kliegl, Marta Stepniewska-Dziubinska, Matvei Novikov, Mehrzad Samadi, Meredith Price, Meriem Boubdir, Michael Boone, Michael Evans, Michal Bien, Michal Zawalski, Miguel Martinez, Mike Chrzanowski, Mohammad Shoeybi, Mostofa Patwary, Namit Dhameja, Nave Assaf, Negar Habibi, Nidhi Bhatia, Nikki Pope,

- Nima Tajbakhsh, Nirmal Kumar Juluru, Oleg Rybakov, Oleksii Hrinchuk, Oleksii Kuchaiev, Oluwatobi Olabiye, Pablo Ribalta, Padmavathy Subramanian, Parth Chadha, Pavlo Molchanov, Peter Dykas, Peter Jin, Piotr Bialecki, Piotr Januszewski, Pradeep Thalasta, Prashant Gaikwad, Prasoon Varshney, Pritam Gundecha, Przemek Tredak, Rabeeh Karimi Mahabadi, Rajen Patel, Ran El-Yaniv, Ranjit Rajan, Ria Cheruvu, Rima Shahbazyan, Ritika Borkar, Ritu Gala, Roger Waleffe, Ruoxi Zhang, Russell J. Hewett, Ryan Prenger, Sahil Jain, Samuel Krizan, Sanjeev Satheesh, Saori Kaji, Sarah Yurick, Saurav Muralidharan, Sean Narenthiran, Seonmyeong Bak, Sepehr Sameni, Seungju Han, Shanmugam Ramasamy, Shaona Ghosh, Sharath Turuvekere Sreenivas, Shelby Thomas, Shizhe Diao, Shreya Gopal, Shrimai Prabhume, Shubham Toshniwal, Shuoyang Ding, Siddharth Singh, Siddhartha Jain, Somshubra Majumdar, Soumye Singhal, Stefania Alborghetti, Syeda Nahida Akter, Terry Kong, Tim Moon, Tomasz Hliwiak, Tomer Asida, Tony Wang, Tugrul Konuk, Twinkle Vashishth, Tyler Poon, Udi Karpas, Vahid Noroozi, Venkat Srinivasan, Vijay Korthikanti, Vikram Fugro, Vineeth Kalluru, Vitaly Kurin, Vitaly Lavrukhin, Wasi Uddin Ahmad, Wei Du, Wonmin Byeon, Ximing Lu, Xin Dong, Yashaswi Karnati, Yejin Choi, Yian Zhang, Ying Lin, Yonggan Fu, Yoshi Suhara, Zhen Dong, Zhiyu Li, Zhongbo Zhu, and Zijia Chen. Nvidia nemotron nano 2: An accurate and efficient hybrid mamba-transformer reasoning model, 2025. <https://arxiv.org/abs/2508.14444>.
- NVIDIA Corporation. *Parallel Thread Execution (PTX ISA)*. NVIDIA. <https://docs.nvidia.com/cuda/parallel-thread-execution/>.
- J. M. Ortega and W. C. Rheinboldt. *Iterative Solution of Nonlinear Equations in Several Variables*. Society for Industrial and Applied Mathematics, 2000. doi: 10.1137/1.9780898719468. <https://epubs.siam.org/doi/abs/10.1137/1.9780898719468>.
- Denis Paperno, Germán Kruszewski, Angeliki Lazaridou, Ngoc-Quan Pham, Raffaella Bernardi, Sandro Pezzelle, Marco Baroni, Gemma Boleda, and Raquel Fernández. The lambada dataset: Word prediction requiring a broad discourse context. In *Proceedings of the 54th annual meeting of the association for computational linguistics (volume 1: Long papers)*, pages 1525–1534, 2016.
- Adam Paszke, Sam Gross, Francisco Massa, Adam Lerer, James Bradbury, Gregory Chanan, Trevor Killeen, Zeming Lin, Natalia Gimelshein, Luca Antiga, et al. Pytorch: An imperative style, high-performance deep learning library. *Advances in neural information processing systems*, 32, 2019.
- Bo Peng, Eric Alcaide, Quentin Anthony, Alon Albalak, Samuel Arcadinho, Stella Biderman, Huanqi Cao, Xin Cheng, Michael Chung, Matteo Grella, et al. Rvk: Reinventing rnns for the transformer era. *arXiv preprint arXiv:2305.13048*, 2023.
- Hao Peng, Nikolaos Pappas, Dani Yogatama, Roy Schwartz, Noah A Smith, and Lingpeng Kong. Random feature attention. *arXiv preprint arXiv:2103.02143*, 2021.
- Korbinian Pöppel, Maximilian Beck, and Sepp Hochreiter. Flashrnn: I/o-aware optimization of traditional rnns on modern hardware, 2025. <https://arxiv.org/abs/2412.07752>.
- Zhen Qin, Songlin Yang, Weixuan Sun, Xuyang Shen, Dong Li, Weigao Sun, and Yiran Zhong. Hgrn2: Gated linear rnns with state expansion. *arXiv preprint arXiv:2404.07904*, 2024.
- Liliang Ren, Yang Liu, Yadong Lu, Yelong Shen, Chen Liang, and Weizhu Chen. Samba: Simple hybrid state space models for efficient unlimited context language modeling. *arXiv preprint arXiv:2406.07522*, 2024.
- Melissa Roemmele, Cosmin Adrian Bejan, and Andrew S. Gordon. Choice of Plausible Alternatives: An Evaluation of Commonsense Causal Reasoning. In *AAAI Spring Symposium on Logical Formalizations of Commonsense Reasoning*, Stanford University, March 2011. <http://ict.usc.edu/pubs/Choice%20of%20Plausible%20Alternatives-%20An%20Evaluation%20of%20Commonsense%20Causal%20Reasoning.pdf>.
- Keisuke Sakaguchi, Ronan Le Bras, Chandra Bhagavatula, and Yejin Choi. Winogrande: An adversarial winograd schema challenge at scale, 2019. <https://arxiv.org/abs/1907.10641>.
- Imanol Schlag, Kazuki Irie, and Jürgen Schmidhuber. Linear transformers are secretly fast weight programmers. In *International conference on machine learning*, pages 9355–9366. PMLR, 2021.
- Jay Shah, Ganesh Bikshandi, Ying Zhang, Vijay Thakkar, Pradeep Ramani, and Tri Dao. Flashattention-3: Fast and accurate attention with asynchrony and low-precision. *Advances in Neural Information Processing Systems*, 37: 68658–68685, 2024.
- Noam Shazeer. Glu variants improve transformer. *arXiv preprint arXiv:2002.05202*, 2020.
- Noam Shazeer, Azalia Mirhoseini, Krzysztof Maziarsz, Andy Davis, Quoc Le, Geoffrey Hinton, and Jeff Dean.

- Outrageously large neural networks: The sparsely-gated mixture-of-experts layer. *arXiv preprint arXiv:1701.06538*, 2017.
- Mohammad Shoeybi, Mostofa Patwary, Raul Puri, Patrick LeGresley, Jared Casper, and Bryan Catanzaro. Megatron-lm: Training multi-billion parameter language models using model parallelism. *arXiv preprint arXiv:1909.08053*, 2019.
- Julien Siems, Timur Carstensen, Arber Zela, Frank Hutter, Massimiliano Pontil, and Riccardo Grazi. Deltaproduct: Improving state-tracking in linear rnns via householder products. *arXiv preprint arXiv:2502.10297*, 2025.
- Shaden Smith, Mostofa Patwary, Brandon Norick, Patrick LeGresley, Samyam Rajbhandari, Jared Casper, Zhun Liu, Shrimai Prabhumoye, George Zerveas, Vijay Korthikanti, et al. Using deepspeed and megatron to train megatron-turing nlg 530b, a large-scale generative language model. *arXiv preprint arXiv:2201.11990*, 2022.
- Jianlin Su, Murtadha Ahmed, Yu Lu, Shengfeng Pan, Wen Bo, and Yunfeng Liu. Roformer: Enhanced transformer with rotary position embedding. *Neurocomputing*, 568:127063, 2024.
- Yutao Sun, Li Dong, Shaohan Huang, Shuming Ma, Yuqing Xia, Jilong Xue, Jianyong Wang, and Furu Wei. Retentive network: A successor to transformer for large language models. *arXiv preprint arXiv:2307.08621*, 2023.
- Yi Tay, Mostafa Dehghani, Dara Bahri, and Donald Metzler. Efficient transformers: A survey, 2022. <https://arxiv.org/abs/2009.06732>.
- Kimi Team, Yifan Bai, Yiping Bao, Guanduo Chen, Jiahao Chen, Ningxin Chen, Ruijue Chen, Yanru Chen, Yuankun Chen, Yutian Chen, et al. Kimi k2: Open agentic intelligence. *arXiv preprint arXiv:2507.20534*, 2025.
- Aleksandar Terzić, Nicolas Menet, Michael Hersche, Thomas Hofmann, and Abbas Rahimi. Structured sparse transition matrices to enable state tracking in state-space models. *arXiv preprint arXiv:2509.22284*, 2025.
- Philippe Tillet, H. T. Kung, and David Cox. Triton: an intermediate language and compiler for tiled neural network computations. In *Proceedings of the 3rd ACM SIGPLAN International Workshop on Machine Learning and Programming Languages*, MAPL 2019, page 10–19, New York, NY, USA, 2019. Association for Computing Machinery. ISBN 9781450367196. doi: 10.1145/3315508.3329973. <https://doi.org/10.1145/3315508.3329973>.
- Ashish Vaswani, Noam Shazeer, Niki Parmar, Jakob Uszkoreit, Llion Jones, Aidan N Gomez, Łukasz Kaiser, and Illia Polosukhin. Attention is all you need. *Advances in neural information processing systems*, 30, 2017.
- Johannes Welbl, Nelson F. Liu, and Matt Gardner. Crowdsourcing multiple choice science questions, 2017. <https://arxiv.org/abs/1707.06209>.
- BigScience Workshop, Teven Le Scao, Angela Fan, Christopher Akiki, Ellie Pavlick, Suzana Ilić, Daniel Hesslow, Roman Castagné, Alexandra Sasha Luccioni, François Yvon, et al. Bloom: A 176b-parameter open-access multilingual language model. *arXiv preprint arXiv:2211.05100*, 2022.
- Ruibin Xiong, Yunchang Yang, Di He, Kai Zheng, Shuxin Zheng, Chen Xing, Huishuai Zhang, Yanyan Lan, Liwei Wang, and Tieyan Liu. On layer normalization in the transformer architecture. In *International conference on machine learning*, pages 10524–10533. PMLR, 2020.
- An Yang, Anfeng Li, Baosong Yang, Beichen Zhang, Binyuan Hui, Bo Zheng, Bowen Yu, Chang Gao, Chengen Huang, Chenxu Lv, et al. Qwen3 technical report. *arXiv preprint arXiv:2505.09388*, 2025.
- Songlin Yang, Bailin Wang, Yikang Shen, Rameswar Panda, and Yoon Kim. Gated linear attention transformers with hardware-efficient training. *arXiv preprint arXiv:2312.06635*, 2023.
- Songlin Yang, Jan Kautz, and Ali Hatamizadeh. Gated delta networks: Improving mamba2 with delta rule. *arXiv preprint arXiv:2412.06464*, 2024a.
- Songlin Yang, Bailin Wang, Yu Zhang, Yikang Shen, and Yoon Kim. Parallelizing linear transformers with the delta rule over sequence length. *Advances in neural information processing systems*, 37:115491–115522, 2024b.
- Ted Zadori, Markus Hoehnerbach, Jay Shah, Timmy Liu, Vijay Thakkar, and Tri Dao. Flashattention-4: Algorithm and kernel pipelining co-design for asymmetric hardware scaling, 2026. <https://arxiv.org/abs/2603.05451>.
- Rowan Zellers, Ari Holtzman, Yonatan Bisk, Ali Farhadi, and Yejin Choi. Hellaswag: Can a machine really finish your sentence?, 2019. <https://arxiv.org/abs/1905.07830>.
- Biao Zhang and Rico Sennrich. Root mean square layer normalization. *Advances in neural information processing systems*, 32, 2019.

A State Size Expansion

Attention Pattern	\mathbf{W}_q	\mathbf{W}_k	\mathbf{W}_v	\mathbf{W}_g	\mathbf{W}_f	\mathbf{W}_o	Total (P)	State Size (NKV)
Multi-Head	NKd_m	NKd_m	NVd_m	NVd_m	Nd_m	NVd_m	$\approx N(2K + 3V)d_m$	$\approx \frac{PKV}{(2K+3V)d_m}$
Multi-Query	NKd_m	Kd_m	Vd_m	NVd_m	Nd_m	NVd_m	$\approx N(K + 2V)d_m$	$\approx \frac{PKV}{(K+2V)d_m}$
Multi-Key	Kd_m	NKd_m	Vd_m	NVd_m	Nd_m	NVd_m	$\approx N(K + 2V)d_m$	$\approx \frac{PKV}{(K+2V)d_m}$
Multi-Value	Kd_m	Kd_m	NVd_m	NVd_m	Nd_m	NVd_m	$\approx 3NVd_m$	$\approx \frac{PK}{3d_m}$

Table 8 Number of parameters in all linear projections. N denotes the number of heads and d_m denotes the model’s embedding dimension. For all our models, we use $K = 64$ and $V = 16$ which results in the largest state size for the multi-value attention formulation for constant number of total parameters (P).

B Representation Power of M²RNN Layers

Theorem 1: The M²RNN recurrence can represent all tasks representable by non-linear vector-valued RNNs and hence can represent regular languages.

Proof. We show that M²RNN can simulate a vector-valued nonlinear RNN, which is known to recognize all regular languages.

Consider the parameter setting

$$f_t = 0, \quad w_r = \mathbf{0}_V, \quad q_t = k_t = e_1 \in \mathbb{R}^K,$$

where $e_1 = [1, 0, \dots, 0]^\top$ is the first standard basis vector.

Under this choice, the matrix-valued recurrence reduces in its first row to

$$\mathbf{Z}_t = \tanh \left(\mathbf{H}_{t-1} \mathbf{W} + \begin{bmatrix} v_t^\top \\ \mathbf{0}_V^\top \\ \vdots \\ \mathbf{0}_V^\top \end{bmatrix} \right), \quad (25)$$

and the output is obtained from the first row,

$$y_t = (\mathbf{Z}_t)_{1,:}$$

This is precisely a standard vector-valued nonlinear RNN with tanh activation applied to the first row of the state matrix. Since vector-valued nonlinear RNNs can represent any regular language, it follows that M²RNN can represent any regular language. \square

C RMSNormTP Module

The forward computation for RMSNorm (Zhang and Sennrich, 2019) applied on the input activations x is given by:

$$s = \frac{1}{\sqrt{\frac{1}{d} \sum_{j=1}^d x_j^2}} \quad (26)$$

$$y_i = (w_i \odot x_i) s \quad (27)$$

where i indicates the i^{th} feature of the input or output, d is the number of features and w is some learnable weight for the RMSNorm module. We cache s during the forward computation in HBM for backward computation. Similarly, the backward computation is given by:

$$p_i = w_i \odot \nabla_{y_i} \mathcal{L} \quad (28)$$

$$r = \sum_{j=1}^d p_j x_j \quad (29)$$

$$\nabla_{x_i} \mathcal{L} = s p_i - \frac{r s^3 x_i}{d} \quad (30)$$

$$\nabla_{w_i} \mathcal{L} = (\nabla_{y_i} \mathcal{L} \odot x_i) s \quad (31)$$

To use RMSNorm (Zhang and Sennrich, 2019) module with M²RNN layers with Tensor Parallelism (TP), we shard the weight w for RMSNorm among the GPUs participating in TP. Since the incoming activations x are also sharded along the feature dimension, to compute the inverse of the normalization term s , we require an AllReduce operation in the forward. We propose the RMSNormTP module which modifies the RMSNorm module to compute s in forward and r in backward as:

$$s = \frac{1}{\sqrt{\frac{1}{d} \sum_{n=1}^{N_{TP}} \sum_{j \in D_n} x_j^2}} \quad (32)$$

$$r = \sum_{n=1}^{N_{TP}} \sum_{j \in D_n} p_j x_j \quad (33)$$

where D_n indicates the sharded features on n^{th} GPU for TP. The summation in blue colour indicates an AllReduce operation across GPUs in Equations 32, 33. Note that for both AllReduce operations, we only need to communicate a single element.